National Nuclear Security Administration

SAND2009-5822
Unlimited Release
Printed September 2009

PAT-1 Safety Analysis Report Addendum

Docket No. 71-0361

Revision 0, September 2009

Prepared by:
Sandia National Laboratories
Albuquerque, New Mexico 87185

Sandia is a multiprogram laboratory operated by Sandia Corporation, a Lockheed Martin Company, for the United States Department of Energy's National Nuclear Security Administration under Contract DE-AC04-94AL85000.

Sandia National Laboratories

Issued by Sandia National Laboratories, operated for the United States Department of Energy by Sandia Corporation.

Available to DOE and DOE contractors from
U.S. Department of Energy
Office of Scientific and Technical Information
P.O. Box 62
Oak Ridge, TN 37831

Telephone: (865) 576-8401
Facsimile: (865) 576-5728
E-Mail: reports@adonis.osti.gov
Online ordering: http://www.osti.gov/bridge

Available to the public from
U.S. Department of Commerce
National Technical Information Service
5285 Port Royal Rd.
Springfield, VA 22161

Telephone: (800) 553-6847
Facsimile: (703) 605-6900
E-Mail: orders@ntis.fedworld.gov
Online order: http://www.ntis.gov/help/ordermethods.asp?loc=7-4-0#online

Sandia
National
Laboratories

SAND2009-5822
Unlimited Release
Printed September 2009

PAT-1 Safety Analysis Report Addendum

Docket No. 71-0361

Revision 0, September 2009

P.O. Box 5800,
Sandia National Laboratories
Albuquerque, NM 87185

Author: Richard H. Yoshimura, David C. Harding, Lili A. Akin, Robert J. Kalan, Carlos Lopez, Perry L. Jones, David R. Miller, David T. Schmale, Gerald A. Knorovsky, Charles W. Morrow, and Ruth F. Weiner

Contributors:
Don Mueller (ORNL), Bryan Broadhead (ORNL), Richard E. Mason (LANL), Stephen P. Willson, LANL), Jim Rubin (LANL), and Michael L. Caviness (LANL)

Abstract

The Plutonium Air Transportable Package, Model PAT-1, is certified under Title 10, Code of Federal Regulations Part 71 by the U.S. Nuclear Regulatory Commission (NRC) per Certificate of Compliance (CoC) USA/0361B(U)F-96 (currently Revision 9). The purpose of this SAR Addendum is to incorporate plutonium (Pu) metal as a new payload for the PAT-1 package. The Pu metal is packed in an inner container (designated the T-Ampoule) that replaces the PC-1 inner container. The documentation and results from analysis contained in this addendum demonstrate that the replacement of the PC-1 and associated packaging material with the T-Ampoule and associated packaging with the addition of the plutonium metal content are not significant with respect to the design, operating characteristics, or safe performance of the containment system and prevention of criticality when the package is subjected to the tests specified in 10 CFR 71.71, 71.73 and 71.74.

This page intentionally left blank

TABLE OF CONTENTS

1. GENERAL INFORMATION 1-1
1.1 Introduction 1-1
1.2 Package Description 1-2
1.2.1 Packaging 1-2
1.2.2 Contents 1-5
1.2.3 Special Requirements for Pu 1-14
1.2.4 Operational Features 1-14
1.3 Appendix 1-15
1.3.1 References 1-15
1.3.2 Drawings 1-15
1.3.3 Specifications 1-43

2. STRUCTURAL EVALUATION 2-1
2.1 Description of Structural Design 2-1
2.1.1 Discussion 2-3
2.1.2 Design Criteria 2-4
2.1.3 Weights and Centers of Gravity 2-9
2.1.4 Identification of Codes and Standards for the Package Design 2-10
2.2 Materials 2-11
2.2.1 Material Properties and Specifications 2-11
2.2.2 Chemical, Galvanic, or Other Reactions 2-11
2.2.3 Effects of Radiation on Materials 2-12
2.3 Fabrication and Examination 2-13
2.3.1 Fabrication 2-13
2.3.2 Examination 2-14
2.4 General Requirements for All Packages 2-14
2.4.1 Minimum Package Size 2-14
2.4.2 Tamper-Indicating Device 2-14
2.4.3 Positive Closure 2-14
2.5 Lifting and Tie-Down Standards for All Packages 2-14
2.5.1 Lifting Devices 2-14
2.5.2 Tie-Down Devices 2-14
2.6 Normal Conditions of Transport 2-14
2.6.1 Heat 2-15
2.6.2 Cold 2-16
2.6.3 Reduced External Pressure 2-17
2.6.4 Increased External Pressure 2-17
2.6.5 Vibration 2-17
2.6.6 Water Spray 2-17
2.6.7 Free Drop 2-17
2.6.8 Corner Drop 2-17
2.6.9 Compression 2-17
2.6.10 Penetration 2-17
2.7 Hypothetical Accident Conditions 2-18

2.7.1 Free Drop 2-18
2.7.2 Crush 2-19
2.7.3 Puncture 2-20
2.7.4 Thermal 2-20
2.7.5 Immersion – Fissile Material 2-21
2.7.6 Immersion – All Packages 2-21
2.7.7 Deep Water Immersion Test (for Type B Packages Containing More than 10^5 A_2) 2-21
2.7.8 Summary of Damage 2-21
2.8 Accident Conditions for Air Transport of Plutonium 2-22
2.8.1 Discussion 2-22
2.8.2 Full Package Validation Model 2-24
2.8.3 Impact Test and Material Failure 2-24
2.8.4 NCT, HAC, and High Velocity Impact Analyses 2-25
2.8.5 Bolt Analysis 2-32
2.8.6 Summary 2-32
2.9 Accident Conditions for Fissile Material Packages for Air Transport 2-33
2.10 Special Form 2-33
2.11 Fuel Rods 2-33
2.12 Appendix 2-33
2.12.1 References 2-33
2.12.2 Full Model Validation Analyses 2-36
2.12.3 Impact Test and Material Failure Criterion 2-49
2.12.4 Material Data 2-75
2.12.5 Component Analyses Using Complete Model 2-93
2.12.6 Bolt Analysis 2-356
2.12.7 Sample Input 2-357
2.12.8 Design Pressure Calculations for the T-Ampoule (in Accordance with Section VIII Division 1 of the ASME Boiler and Pressure Vessel Code 2-377

3. THERMAL EVALUATION 1
3.1 Description of Thermal Design 1
3.1.1 Design Features 2
3.1.2 Decay Heat of the Contents 2
3.1.3 Summary Tables of Temperatures 4
3.1.4 Summary Table of Maximum Pressures 4
3.2 Material Properties and Component Specifications 5
3.2.1 Material Properties 5
3.2.2 Component Specifications 6
3.3 Thermal Evaluation under NCT 7
3.3.1 Heat and Cold 10
3.3.2 Maximum Normal Operating Pressure 15
3.4 Thermal Evaluation under HAC 16
3.4.1 Initial Conditions 21
3.4.2 Hypothetical Accident Conditions (HAC) 21
3.4.3 Maximum Temperatures and Pressure 25

3.4.4 Maximum Thermal Stresses 27
3.4.5 Hypothetical Accident Conditions for Fissile Material Packages for Air Transport 28
3.5 Appendix 30
3.5.1 References 30
3.5.2 Parker O-Ring Data Sheet 31
3.5.3 Eutectic Analysis of Ti-6Al-4V with Plutonium and Copper 34

4. CONTAINMENT 1
4.1 Description of the Containment System 2
4.1.1 Special Requirements for Plutonium 3
4.1.2 Plutonium Metal Contents 5
4.2 Containment under Normal Conditions of Transport (NCT) 8
4.3 Containment under Hypothetical Accident Conditions (HAC) 9
4.3.1 Containment under Plutonium Air Transport Fire Test 9
4.4 Leakage Rate Tests for Type B Packages 10
4.5 Appendix 11
4.5.1 References 11
4.5.2 PAT-1 Contents 12
4.5.3 Helium Generation 19
4.5.4 O-Ring Decomposition 24

5. SHIELDING EVALUATION 5-1
5.1 Description of Shielding Design 5-1
5.1.1 Design Features 5-1
5.1.2 Summary Table of Maximum Radiation Levels 5-2
5.2 Source Specification 5-2
5.2.1 Gamma Source 5-3
5.2.2 Neutron Source 5-3
5.3 Shielding Model 5-4
5.3.1 Configuration of Source and Shielding 5-4
5.3.2 Material Properties 5-6
5.4 Shielding Evaluation 5-7
5.4.1 Methods 5-7
5.4.2 Input and Output Data 5-10
5.4.3 Flux-to-Dose-Rate Conversion 5-11
5.4.4 External Radiation Levels 5-11
5.5 Appendix 5-15
5.5.1 References 5-15
5.5.2 Summary of Source Bounding Analyses 5-15
5.5.3 Analysis of Pu/Be Source Contents 5-19
5.5.4 List of Various Code Inputs 5-24

6. CRITICALITY EVALUATION 6-1
6.1 Description of Criticality Design 6-1
6.1.1 Design Features 6-1

6.1.2 Summary Table of Criticality Evaluation 6-2
6.1.3 Criticality Safety Index 6-2
6.2 Fissile Material Contents 6-3
6.2.1 Plutonium Metal – General Form 6-3
6.2.2 Plutonium Metal – Pu/Be Sources 6-4
6.3 General Considerations 6-4
6.3.1 Model Configuration 6-4
6.3.2 Material Properties 6-11
6.3.3 Computer Codes and Cross-Section Libraries 6-16
6.3.4 Demonstration of Maximum Reactivity 6-17
6.4 Single Package Evaluation 6-39
6.4.1 Configuration 6-39
6.4.2 Results 6-40
6.5 Evaluation of Package Arrays under Normal Conditions of Transport 6-40
6.5.1 Configuration 6-40
6.5.2 Results 6-40
6.6 Package Arrays under Hypothetical Accident Conditions 6-40
6.6.1 Configuration 6-40
6.6.2 Results 6-41
6.7 Fissile Material Packages for Air Transport 6-41
6.7.1 Configuration 6-41
6.7.2 Results 6-41
6.8 Benchmark Evaluations 6-41
6.8.1 Applicability of Benchmark Experiments 6-42
6.8.2 Bias Determination 6-48
6.9 Appendices 6-59
6.9.1 References 6-59
6.9.2 TB-1 Containment Vessel Inner Volume 6-62
6.9.3 Applicability of Benchmark Experiments 6-63
6.9.4 Calculation Results 6-76
6.9.5 Sample inputs 6-109
6.9.6 Considerations for Pu/Be Sources 6-116

7. PACKAGE OPERATIONS 7-1
7.1 Package Loading 7-1
7.1.1 Preparation for Loading 7-2
7.1.2 Loading of Contents 7-5
7.1.3 Preparation for Transport 7-17
7.2 Package Unloading 7-20
7.2.1 Receipt of Package from Carrier 7-20
7.2.2 Removal of Contents 7-21
7.3 Preparation of Empty Package for Transport 7-25
7.3.1 Transporting the PAT-1 Package with an Empty T-Ampoule 7-25
7.3.2 Transporting an Empty PAT-1 package without a T-Ampoule 7-26
7.4 Other Operations 7-27
7.5 Appendix 7-27

7.5.1 References 7-27

8. ACCEPTANCE TESTS AND MAINTENANCE PROGRAM 8-1
8.1 Acceptance Tests 8-1
8.1.1 Visual Inspections and Measurements 8-2
8.1.2 Weld Examinations 8-2
8.1.3 Structural and Pressure Tests 8-2
8.1.4 Leakage Tests 8-5
8.1.5 Component and Material Tests 8-5
8.1.6 Shielding Tests 8-6
8.1.7 Thermal Tests 8-6
8.1.8 Miscellaneous Tests 8-6
8.2 Maintenance Program 8-6
8.2.1 Structural and Pressure Tests 8-7
8.2.2 Leakage Tests 8-7
8.2.3 Component and Material Tests 8-7
8.2.4 Thermal Tests 8-7
8.2.5 Miscellaneous Tests 8-7
8.3 Appendix 8-8
8.3.1 References 8-8

9. QUALITY ASSURANCE 9-1
9.1 Organization 9-1
9.2 Quality Assurance Program 9-3
9.2.1 General 9-3
9.2.2 QA Levels 9-7
9.3 Package Design Control 9-10
9.4 Procurement Document Control 9-11
9.5 Instructions, Procedures, and Drawings 9-12
9.5.1 Operating Procedures for Preparation and Use of Packaging System 9-13
9.5.2 Operating Procedure Changes 9-13
9.6 Document Control 9-13
9.7 Control of Purchased Material, Equipment, and Services 9-14
9.8 Identification and Control of Material, Parts, and Components 9-15
9.9 Control of Special Processes 9-16
9.10 Internal Inspection 9-17
9.10.1 Inspections During Fabrication 9-18
9.10.2 Inspections during Initial Acceptance and during Service Life 9-19
9.11 Test Control 9-19
9.11.1 Acceptance Tests 9-20
9.11.2 Maintenance Tests 9-20
9.11.3 Preshipment Tests 9-20
9.12 Control of Measuring and Test Equipment 9-20
9.13 Handling, Storage, and Shipping Control 9-21
9.14 Inspection, Test, and Operating Status 9-21
9.15 Nonconforming Materials, Parts, or Components 9-22

9.16 Corrective Action 9-24
9.17 Quality Assurance Records 9-24
9.17.1 Subcontractor/Supplier Submittal Requirements Summary 9-25
9.18 Audits 9-26
9.19 Appendix 9-26
9.19.1 References 9-26

LIST OF FIGURES

Figure 1-1. Assembled PAT-1 Showing AQ-1, TB-1, and T-Ampoule 1-3
Figure 1-2. T-Ampoule within the TB-1 1-4
Figure 1-3. Two Sample Containers (SC-2) Nested within T-Ampoule and TB-1 1-6
Figure 1-4. Three Sample Containers (SC-1) Nested within T-Ampoule and TB-1 1-7
Figure 1-5. 831 gram (1.83 lb) Pu Hollow Cylinder within T-Ampoule and TB-1 1-8

Figure 2-1. Locus in Equivalent Plastic Strain–Stress Triaxiality Space Developed from Titanium Impact Test 2-8
Figure 2-2. Center of Gravity for PAT-1. (Note That the Center of Gravity Varies with the Inclusion of the Support Structure and Could Vary Because of the Natural Weight Variation of the Kiln-Dried Redwood.) 2-10
Figure 2-3. Flowchart of PAT-1 Analyses 2-23
Figure 2-4. Strain Locus Developed from Titanium Experiment and Finite Element Model 2-25
Figure 2-5. Summary of Highest Tearing Parameter versus Plastic Strain Elements for HAC and High Velocity Analyses 2-29
Figure 2-6. Summary of B-W Strain Locus Values for the Highest Tearing Parameter Elements. 2-29
Figure 2-7. Finite Element Model of the Complete PAT-1 Package 2-36
Figure 2-8. Details of the High-Velocity Finite Element Validation Model 2-37
Figure 2-9. Redwood Force-Deflection Curve Used in Orthotropic Crush Model 2-38
Figure 2-10. Model Slice Configuration for the Orthotropic Crush Material Model 2-40
Figure 2-11. Deformation from an End-On Impact of 445 ft/sec 2-42
Figure 2-12. PAT-1 Dimensions Following 422-FPS Top End Impact (from SAR Figure 2.18) 2-42
Figure 2-13. Full Model TB-1 Deceleration Curve for End-On Impact Analysis (10 CFR 71.74) 2-43
Figure 2-14. Deformation of the Full Package Model after a Side Impact of 445 ft/sec 2-43
Figure 2-15. PAT-1 Dimensions Following 445 FPS Side Impact (from SAR Figure 2.242) 2-44
Figure 2-16. Full Model TB-1 Deceleration Curve for Side Impact Analysis (10 CFR 71.74) 2-44
Figure 2-17. Deformation of the Full Package Model after a CGOC Impact of 445 ft/sec ... 2-45
Figure 2-18. PAT-1 Dimensions Following 443-FPS Bottom Corner Impact (CGOC) (from SAR Figure 2.27 SAR1) 2-45
Figure 2-19. Full Model TB-1 Deceleration Curve for CGOC Impact Analysis (10 CFR 71.74) 2-46

Figure 2-20. NCT and HAC Package Model with Lid Flange 2-47
Figure 2-21. Flange Details of NCT Model (Dimensions in Inches) 2-47
Figure 2-22. Experimental Concept1 2-49
Figure 2-23. Cross-Section of Impactor Assembly and TB-1/Ampoule Assembly 2-50
Figure 2-24. Complete Test Assembly Prior to the Test 2-51
Figure 2-25. (a) Titanium Ampoule and TB-1 Fixture Attached to Actuator Sled; (b) View of Suspended Impactor 2-51
Figure 2-26. DT-45 Drop Table Shock Machine 2-52
Figure 2-27. Solid model of the Ampoule Test Assemble for Drop Table Tests 2-52
Figure 2-28. Photograph of Ampoule Test Assembly Prior to Testing 2-53
Figure 2-29. Finite Element Model for the Brass Impact Test 2-54
Figure 2-30. Equivalent Plastic Strain in the Ampoule Dish at an Impact Velocity of 175 ft/sec 2-54
Figure 2-31. Deformed Shape of and Plastic Strain in the Brass-Tipped Impactor at an Impact Velocity of 175 ft/sec 2-55
Figure 2-32. Deformed Shape of the Brass Impactor Overlaid on the Test Specimen 2-55
Figure 2-33. Comparison of the Brass-Tipped Impactor Acceleration from the Test and the Finite Element Model 2-56
Figure 2-34. Deformed Mesh of the Titanium Tipped Impactor, at an Impact Velocity of 200 ft/sec 2-57
Figure 2-35. Equivalent Plastic Strain in the Ampoule Dish at an Impact Velocity of 200 ft/sec with a Titanium Tipped Impactor 2-57
Figure 2-36. Deformed Finite Element Mesh of Titanium Impactor with Contours of Equivalent Plastic Strain 2-58
Figure 2-37. Deformed Shape of the Titanium Impactor Overlaid on the Test Specimen 2-58
Figure 2-38. Finite Element Model of the Drop Table Ampoule Test 2-59
Figure 2-39. Drop Table Acceleration 2-60
Figure 2-40. Finite Element Results Showing the Deformed Shape of the Ampoule Test Specimen 2-60
Figure 2-41. Photographs of the Deformed Ampoule Specimen (a) Top View (b) Inner Surface 2-61
Figure 2-42. Maximum Equivalent Plastic Strain in Sample Test Specimen 2-61
Figure 2-43. Nominal Element Radial Strain Compared to Strain Gage Data 2-62
Figure 2-44. Crush Plate Acceleration 2-62
Figure 2-45. Plastic Strain versus Stress Triaxiality from Johnson and Cook 2-64
Figure 2-46. Stress Failure Locus of Al2024-T351 Developed from Bao 2-64
Figure 2-47. General Failure Locus of Ductile Metals Developed by Bao and Wierzbicki. . 2-65
Figure 2-48. Equivalent Plastic Strain in the Titanium Tip for an Impact Velocity of 200 ft/sec 2-66
Figure 2-49. Equivalent Plastic Strain in the Titanium Ampoule in the Drop Table Test 2-67
Figure 2-50. Locus in Equivalent Plastic Strain–Stress Triaxiality Space Developed from Titanium Impact Tests 2-67
Figure 2-51. Stress Triaxiality and Equivalent Plastic Strain versus Time for Element 46152 2-68
Figure 2-52. Stress Triaxiality and Average Stress Triaxiality as a Function of Equivalent Plastic Strain for Element 46152 2-69

Figure 2-53. Finite Element Model of Titanium Tensile Test Specimen (a) Original Mesh (b) Deformed Mesh (c) Equivalent Plastic Strain 2-70
Figure 2-54. Stress Triaxiality and Equivalent Plastic Strain versus Displacement for Center Element 2-70
Figure 2-55. Stress Triaxiality and Average Stress Triaxiality as a Function of Plastic Strain for the Highest Stressed Element 2-71
Figure 2-56. Tensile Test Results Showing Peak Value of Failure Parameter TP 2-72
Figure 2-57. Redwood Force Deflection Curve Compared to Test Data from Joseph and Hill 2-76
Figure 2-58. Comparison of Power-Law Curve Fit with Data from Tensile Test 2-84
Figure 2-59. Effect of Temperature on the Tensile Ultimate Strength and Tensile Yield Strength of Annealed Ti-6-Al-4V Alloy (Ref. 2, Taken from MIL-HDBK-5E, Figure 5.4.1.1.1.1) 2-85
Figure 2-60. Effect of Temperature on the Elongation of Annealed Ti-6-Al-4V Alloy (Ref. 2, Taken from MIL-HDBK-5E, Figure 5.4.1.1.5) 2-85
Figure 2-61. Pu Stress-Strain Curves Taken from Hecker and Stevens [Figure 2(a)] 2-87
Figure 2-62. Pu Stress-Strain Curves Taken from Hecker and Stevens (Figure 10[b]). 2-88
Figure 2-63. Comparison of Power-Law Curve Fit with Data from Tensile Test 2-91
Figure 2-64. Comparison of Power-Law Curve Fit with Data from Tensile Test 2-92
Figure 2-65. Common Components of the Model for Top and CGOC Impact Orientation .. 2-95
Figure 2-66. Common Components of the Model for a Side Impact Orientation 2-95
Figure 2-67. Support Structure with 0° Rotation and Spacers for SC-1 2-96
Figure 2-68. Support Structure with 45° Rotation and Spacer for SC-2 2-96
Figure 2-69. Mesh Refinement in Support Structure with 0° Rotation and Spacer for SC-1 2-97
Figure 2-70. 831-g Cylinder Finite Element Model 2-98
Figure 2-71. 731-g Cylinder Finite Element Model 2-98
Figure 2-72. Finite Element Model of SC-1 with Pu Cylinder Contents 2-99
Figure 2-73. Finite Element Model of SC-2 with Pu Cylinder Contents 2-99
Figure 2-74. NCT SC-2 Side Impact with Support Structure Rotated 45° 2-100
Figure 2-75. NCT SC-1 Side Impact with Support Structure Rotated 0° 2-101
Figure 2-76. NCT SC-1 End Impact with Support Structure Rotated 0° 2-101
Figure 2-77. NCT SC-2 End Impact with Support Structure Rotated 0° 2-102
Figure 2-78. NCT SC-1 End Impact with Support Structure Rotated 0° – Final Displacement 2-103
Figure 2-79. NCT SC-2 End Impact with Support Structure Rotated 0° – Final Displacement 2-103
Figure 2-80. NCT SC-1 End Impact with Support Structure Rotated 0° - Kinetic Energy Time History 2-104
Figure 2-81. NCT SC-2 End Impact with Support Structure Rotated 0° - Kinetic Energy Time History 2-104
Figure 2-82. NCT SC-1 End Impact with Support Structure Rotated 0° - EQPS in Bottom Legs 2-105
Figure 2-83. NCT SC-1 End Impact with Support Structure Rotated 0° - EQPS in Top Legs 2-105
Figure 2-84. NCT SC-1 End Impact with Support Structure Rotated 0° – EQPS in Top Dish 2-106

Figure 2-85. NCT SC-2 End Impact with Support Structure Rotated 0° – EQPS in Bottom Legs 2-106
Figure 2-86. NCT SC-2 End Impact with Support Structure Rotated 0° – EQPS in Top Dish 2-107
Figure 2-87. NCT SC-1 Side Impact with Support Structure Rotated 45° 2-108
Figure 2-88. NCT SC-2 Side Impact with Support Structure Rotated 0° 2-108
Figure 2-89. NCT SC-1 Side Impact with Support Structure Rotated 45° – Final Displacement 2-109
Figure 2-90. NCT SC-1 Side Impact with Support Structure Rotated 0° – Final Displacement 2-109
Figure 2-91. NCT SC-2 Side Impact with Support Structure Rotated 45° – Final Displacement 2-110
Figure 2-92. NCT SC-2 Side Impact with Support Structure Rotated 0° - Final Displacement 2-110
Figure 2-93. NCT SC-1 Side Impact with Support Structure Rotated 45° - Kinetic Energy Time History 2-111
Figure 2-94. NCT SC-2 Side Impact with Support Structure Rotated 45° - Kinetic Energy Time History 2-111
Figure 2-95. NCT SC-1 Side Impact with Support Structure Rotated 0° – Kinetic Energy Time History 2-112
Figure 2-96. NCT SC-2 Side Impact with Support Structure Rotated 0° – Kinetic Energy Time History 2-112
Figure 2-97. NCT SC-1 Side Impact with Support Structure Rotated 45° – EQPS in Bottom Dish 2-113
Figure 2-98. NCT SC-1 Side Impact with Support Structure Rotated 45° – EQPS in Top Legs 2-113
Figure 2-99. NCT SC-1 Side Impact with Support Structure Rotated 45° – EQPS in Top Dish 2-114
Figure 2-100. NCT SC-2 Side Impact with Support Structure Rotated 45° – EQPS in Bottom Dish 2-114
Figure 2-101. NCT SC-2 Side Impact with Support Structure Rotated 45° – EQPS in Top Legs 2-115
Figure 2-102. NCT SC-2 Side Impact with Support Structure Rotated 45° – EQPS in Top Dish 2-115
Figure 2-103. NCT SC-1 Side Impact with Support Structure Rotated 0° – EQPS in Bottom Legs 2-116
Figure 2-104. NCT SC-1 Side Impact with Support Structure Rotated 0° – EQPS in Top Dish 2-116
Figure 2-105. NCT SC-2 Side Impact with Support Structure Rotated 0° – EQPS in Bottom Legs 2-117
Figure 2-106. NCT SC-2 Side Impact with Support Structure Rotated 45° - EQPS in T-Ampoule 2-118
Figure 2-107. NCT SC-2 Side Impact with Support Structure Rotated 45° - EQPS in TB-1 2-118
Figure 2-108. NCT SC-2 Side Impact with Support Structure Rotated 45° - Tresca Stress in TB-1 2-119

Figure 2-109. Finite Element Mesh for the 831-g, Plutonium Metal Hollow Cylinder, Bottom Position, End Impact 2-123
Figure 2-110. Finite Element Mesh for the 831-g, Plutonium Metal Hollow Cylinder, Bottom Position, End Impact – Final Displacement 2-123
Figure 2-111. Kinetic Energy Time History for the 831-g, ER Cylinder, Bottom Position, End Impact 2-124
Figure 2-112. EQPS in the TB-1 for the 831-g, ER Cylinder, Bottom Position, End Impact 2-124
Figure 2-113. EQPS in TB-1 (Range Zoomed in to Show All Elements with non-zero EQPS) for the 831-g, Hollow Cylinder, Bottom Position, End Impact 2-125
Figure 2-114. von Mises Stress in the TB-1 for the 831-g Plutonium Metal Hollow Cylinder, Bottom Position, End Impact (Rotated Forward for Ease of Viewing) 2-125
Figure 2-115. von Mises Stress in the TB-1 for the 831-g, Plutonium Metal Hollow Cylinder, Bottom Position, End Impact (Rotated Backward for Ease of Viewing) 2-126
Figure 2-116. Summed Contact Force on the TB-1 Top for a 831-g, Plutonium Metal Hollow Cylinder, Top Impact 2-126
Figure 2-117. Finite Element Mesh for the 831-g, Angled, ER Cylinder, Bottom Position, End Impact 2-127
Figure 2-118. Finite Element Mesh for the 831-g, Angled, ER, Cylinder, Bottom Position, End Impact – Final Displacement 2-128
Figure 2-119. Kinetic Energy Time History for the 831-g, Angled, Plutonium Metal Hollow Cylinder, Bottom Position, End Impact 2-128
Figure 2-120. Graph of Average Stress Triaxiality versus EQPS of Elements Exceeding the Experimental Strain Locus for the 831-g, Angled, Plutonium Metal Hollow Cylinder, Bottom Position, End Impact 2-129
Figure 2-121. Graph of Average Stress Triaxiality versus EQPS of Elements Exceeding the Experimental Strain Locus (Zoomed In) for the 831-g, Angled, Plutonium Metal Hollow Cylinder, Bottom Position, End Impact 2-129
Figure 2-122. Graph of Tearing Parameter versus EQPS for Elements Exceeding the Experimental Strain Locus for the 831-g, Angled, Plutonium Metal Hollow Cylinder, Bottom Position, End Impact 2-130
Figure 2-123. Plot of Elements Exceeding the Experimental Strain Locus for the 831-g, Angled, Plutonium Metal Hollow Cylinder, Bottom Position, End Impact 2-130
Figure 2-124. Plot of EQPS in the TB-1 for the 831-g Angled, ER, Cylinder, Bottom Position, End Impact 2-131
Figure 2-125. Plot of EQPS in the TB-1 (Range Zoomed in to Show all Elements with Non-Zero EQPS) for the 831-g, Angled, Plutonium Metal Hollow Cylinder, Bottom Position, End Impact 2-131
Figure 2-126. Plot of von Mises Stress in the TB-1 for the 831-g, Angled, Plutonium Metal Hollow Cylinder, Bottom Position, End Impact 2-132
Figure 2-127. Plot of von Mises Stress in the TB-1 for the 831-g, Angled, Plutonium Metal Hollow Cylinder, Bottom Position, End Impact 2-132
Figure 2-128. Plot of Contact Force in the TB-1 for the 831-g, Angled Plutonium Metal Hollow Cylinder, Bottom Position, End Impact 2-133

Figure 2-129. Finite Element Mesh for the 831-g, Angled, ER Cylinder, Bottom Position, CGOC Impact 2-134
Figure 2-130. Finite Element Mesh for the 831-g, Angled, ER Cylinder, Bottom Position, CGOC Impact – Final Displacement 2-135
Figure 2-131. Kinetic Energy Time History for the 831-g, Angled, Plutonium Metal Hollow Cylinder, Bottom Position, CGOC Impact 2-135
Figure 2-132. Graph of Average Stress Triaxiality versus EQPS of Elements Exceeding the Experimental Strain Locus for the 831-g, Angled, Plutonium Metal Hollow Cylinder, Bottom Position, CGOC Impact 2-136
Figure 2-133. Graph of Average Stress Triaxiality versus EQPS of Elements Exceeding the Experimental Strain Locus (Zoomed in) for the 831-g, Angled, Plutonium Metal Hollow Cylinder, Bottom Position, CGOC Impact 2-136
Figure 2-134. Graph of Tearing Parameter versus EQPS of Elements Exceeding the Experimental Strain Locus for the 831-g Angled, Plutonium Metal Hollow Cylinder, Bottom Position, CGOC Impact 2-137
Figure 2-135. Plot of Elements Exceeding the Experimental Strain Locus for the 831-g, Angled, Plutonium Metal Hollow Cylinder, Bottom Position, CGOC Impact 2-137
Figure 2-136. Plot of Elements Exceeding the Experimental Strain Locus for the 831-g, Angled, Plutonium Metal Hollow Cylinder, Bottom Position, CGOC Impact 2-138
Figure 2-137. Plot of Elements Exceeding the Experimental Strain Locus for the 831-g, Angled, Plutonium Metal Hollow Cylinder, Bottom Position, CGOC Impact 2-138
Figure 2-138. Plot of EQPS in the TB-1 for the 831-g, Angled, Plutonium Metal Hollow Cylinder, Bottom Position, CGOC Impact 2-139
Figure 2-139. Plot of EQPS in the TB-1 for the 831-g, Angled, Plutonium Metal Hollow Cylinder, Bottom Position, CGOC Impact 2-139
Figure 2-140. Plot of von Mises Stress in the TB-1 for the 831-g, Angled, Plutonium Metal Hollow Cylinder, Bottom Position, CGOC Impact 2-140
Figure 2-141. Finite Element Mesh for the 831-g, ER, Cylinder, Far Side Position, Side Impact 2-141
Figure 2-142. Finite Element Mesh for the 831-g, Plutonium Metal Hollow Cylinder, Far Side Position, Side Impact – Final Displacement 2-141
Figure 2-143. Kinetic Energy Time History for the 831-g, ER, Cylinder, Far Side Position, Side Impact 2-142
Figure 2-144. Graph of Stress Triaxiality versus EQPS of Elements Exceeding the Experimental Strain Locus for the 831-g, Plutonium Metal Hollow Cylinder, Far Side Position, Side Impact 2-142
Figure 2-145. Graph of Stress Triaxiality versus EQPS of Elements Exceeding the Experimental Strain Locus (Zoomed In) for the 831-g, Plutonium Metal Hollow Cylinder, Far Side Position, Side Impact 2-143
Figure 2-146. Graph of Tearing Parameter versus EQPS of Elements Exceeding the Experimental Strain Locus for the 831-g, Plutonium Metal Hollow Cylinder, Far Side Position, Side Impact 2-143
Figure 2-147. Plot of Elements Exceeding the Experimental Strain Locus for the 831-g, Plutonium Metal Hollow Cylinder, Far Side Position, Side Impact 2-144
Figure 2-148. Plot of Elements Exceeding the Experimental Strain Locus for the 831-g, Plutonium Metal Hollow Cylinder, Far Side Position, Side Impact 2-144

Figure 2-149. Plot of EQPS in the TB-1 for the 831-g, ER, Cylinder, Far Side Position, Side Impact 2-145
Figure 2-150. Plot of EQPS in the TB-1 for the 831-g, ER Cylinder, Far Side Position, Side Impact 2-145
Figure 2-151. Plot of von Mises Stress in the TB-1 for the 831-g, ER Cylinder, Far Side Position, Side Impact 2-146
Figure 2-152. Plot of von Mises Stress in the TB-1 for the 831-g, ER, Cylinder, Far Side Position, Side Impact 2-146
Figure 2-153. Finite Element Mesh for the 831-g, Angled, ER Cylinder, Far Side Position, Side Impact 2-147
Figure 2-154. Finite Element Mesh for the 831-g, Angled, ER Cylinder, Far Side Position, Side Impact – Final Displacement 2-148
Figure 2-155. Kinetic Energy Time History for the 831-g, Angled, Plutonium Metal Hollow Cylinder, Far Side Position, Side Impact 2-148
Figure 2-156. Graph of Average Stress Triaxiality versus EQPS of Elements Exceeding the Experimental Strain Locus for the 831-g, Angled, Plutonium Metal Hollow Cylinder, Far Side Position, Side Impact 2-149
Figure 2-157. Graph of Average Stress Triaxiality versus EQPS of Elements Exceeding the Experimental Strain Locus (Zoomed In) for the 831-g, Angled, Plutonium Metal Hollow Cylinder, Far Side Position, Side Impact 2-149
Figure 2-158. Graph of Tearing Parameter versus EQPS of Elements Exceeding the Experimental Strain Locus for the 831-g, Angled, Plutonium Metal Hollow Cylinder, Far Side Position, Side Impact 2-150
Figure 2-159. Plot of Elements Exceeding the Experimental Strain Locus for the 831-g, Angled, Plutonium Metal Hollow Cylinder, Far Side Position, Side Impact .. 2-151
Figure 2-160. Plot of EQPS in the TB-1 for the 831-g, Angled, ER Cylinder, Far Side Position, Side Impact 2-152
Figure 2-161. Plot of EQPS in the TB-1 for the 831-g, Angled, ER Cylinder, Far Side Position, Side Impact 2-152
Figure 2-162. Plot of von Mises Stress in the TB-1 for the 831-g, Angled, Plutonium Metal Hollow Cylinder, Far Side Position, Side Impact 2-153
Figure 2-163. Plot of von Mises Stress in the TB-1 for the 831-g, Angled, Plutonium Metal Hollow Cylinder, Far Side Position, Side Impact 2-153
Figure 2-164. Finite Element Mesh for the 731-g, ER, Cylinder, Bottom Position, Top Impact 2-154
Figure 2-165. Finite Element Mesh for the 731-g, ER, Cylinder, Bottom Position, Top Impact – Final Displacement 2-155
Figure 2-166. Kinetic Energy Time History for the 731-g, ER, Cylinder, Bottom Position, Top Impact 2-155
Figure 2-167. EQPS in the TB-1 for the 731-g, Plutonium Metal Hollow Cylinder, Bottom Position, Top Impact 2-156
Figure 2-168. von Mises Stress in the TB-1 for the 731-g, ER, Cylinder, Bottom Position, Top Impact 2-156
Figure 2-169. von Mises Stress in the TB-1 for the 731-g, ER, Cylinder, Bottom Position, Top Impact 2-157

Figure 2-170. Contact Forces in the TB-1 for the 731-g, ER, Cylinder, Bottom Position, Top Impact 2-157
Figure 2-171. Finite Element Mesh for the 731-g, Angled, ER Cylinder, Bottom Position, Top Impact 2-158
Figure 2-172. Finite Element Mesh for the 731-g, Angled, ER Cylinder, Bottom Position, Top Impact – Final Displacement 2-159
Figure 2-173. Kinetic Energy Time History for the 731-g, Angled, Plutonium Metal Hollow Cylinder, Bottom Position, Top Impact 2-159
Figure 2-174. Graph of Average Stress Triaxiality versus EQPS of Elements Exceeding the Experimental Strain Locus for the 731-g, Angled, Plutonium Metal Hollow Cylinder, Bottom Position, Top Impact 2-160
Figure 2-175. Graph of Average Stress Triaxiality versus EQPS of Elements Exceeding the Experimental Strain Locus (Zoomed In) for the 731-g, Angled, Plutonium Metal Hollow Cylinder, Bottom Position, Top Impact 2-160
Figure 2-176. Graph of Tearing Parameter versus EQPS of Elements Exceeding the Experimental Strain Locus for the 731-g, Angled, Plutonium Metal Hollow Cylinder, Bottom Position, Top Impact 2-161
Figure 2-177. Plot of Elements Exceeding the Experimental Strain Locus for the 731-g, Angled, Plutonium Metal Hollow Cylinder, Bottom Position, Top Impact 2-161
Figure 2-178. Plot of EQPS in the TB-1 for the 731-g, Angled, Plutonium Metal Hollow Cylinder, Bottom Position, Top Impact 2-162
Figure 2-179. Plot of von Mises Stress for the 731-g, Angled, Plutonium Metal Hollow Cylinder, Bottom Position, Top Impact 2-162
Figure 2-180. Plot of von Mises Stress for the 731-g, Angled, Plutonium Metal Hollow Cylinder, Bottom Position, Top Impact 2-163
Figure 2-181. Plot of Contact Force for the 731-g, Angled, Plutonium Metal Hollow Cylinder, Bottom Position, Top Impact 2-163
Figure 2-182. Finite Element Mesh for the 731-g, Angled, Plutonium Metal Hollow Cylinder, Bottom Position, CGOC Impact 2-164
Figure 2-183. Finite Element Mesh for the 731-g, Angled, Plutonium Metal Hollow Cylinder, Bottom Position, CGOC Impact – Final Displacement 2-165
Figure 2-184. Kinetic Energy Time History for the 731-g, Angled, Plutonium Metal Hollow Cylinder, Bottom Position, CGOC Impact 2-165
Figure 2-185. Graph of Average Stress Triaxiality versus EQPS of Elements Exceeding the Experimental Strain Locus for the 731-g, Angled, Plutonium Metal Hollow Cylinder, Bottom Position, CGOC Impact 2-166
Figure 2-186. Graph of Average Stress Triaxiality versus EQPS of Elements Exceeding the Experimental Strain Locus (Zoomed In) for the 731-g, Angled, Plutonium Metal Hollow Cylinder, Bottom Position, CGOC Impact 2-166
Figure 2-187. Graph of Tearing Parameter versus EQPS of Elements Exceeding the Experimental Strain Locus for the 731-g, Angled, Plutonium Metal Hollow Cylinder, Bottom Position, CGOC Impact 2-167
Figure 2-188. Plot of Elements Exceeding the Experimental Strain Locus for the 731-g, Angled, Plutonium Metal Hollow Cylinder, Bottom Position, CGOC Impact 2-167

Figure 2-189. Plot of Elements Exceeding the Experimental Strain Locus for the 731-g, Angled, Plutonium Metal Hollow Cylinder, Bottom Position, CGOC Impact 2-168
Figure 2-190. Plot of EQPS in the TB-1 for the 731-g, Angled, Plutonium Metal Hollow Cylinder, Bottom Position, CGOC Impact 2-168
Figure 2-191. Plot of von Mises Stress in the TB-1 for the 731-g, Angled, Plutonium Metal Hollow Cylinder, Bottom Position, CGOC Impact 2-169
Figure 2-192. Finite Element Mesh for the 731-g, ER, Cylinder, Far Side Position, Side Impact 2-170
Figure 2-193. Finite Element Mesh for the 731-g, Plutonium Metal Hollow Cylinder, Far Side Position, Side Impact – Final Displacement 2-170
Figure 2-194. Kinetic Energy Time History for the 731-g, ER, Cylinder, Far Side Position, Side Impact 2-171
Figure 2-195. Graph of Average Stress Triaxiality versus EQPS of Elements Exceeding the Experimental Strain Locus for the 731-g, Plutonium Metal Hollow Cylinder, Far Side Position, Side Impact 2-171
Figure 2-196. Graph of Average Stress Triaxiality versus EQPS of Elements Exceeding the Experimental Strain Locus (Zoomed In) for the 731-g, Plutonium Metal Hollow Cylinder, Far Side Position, Side Impact 2-172
Figure 2-197. Graph of Tearing Parameter versus EQPS of Elements Exceeding the Experimental Strain Locus for the 731-g, Plutonium Metal Hollow Cylinder, Far Side Position, Side Impact 2-172
Figure 2-198. Plot of Elements Exceeding the Experimental Strain Locus for the 731-g, Plutonium Metal Hollow Cylinder, Far Side Position, Side Impact 2-173
Figure 2-199. Plot of EQPS in the TB-1 for the 731-g, ER Cylinder, Far Side Position, Side Impact 2-173
Figure 2-200. Plot of EQPS in the TB-1 for the 731-g, ER Cylinder, Far Side Position, Side Impact 2-174
Figure 2-201. Plot of EQPS in the TB-1 for the 731-g, ER Cylinder, Far Side Position, Side Impact 2-174
Figure 2-202. Plot of EQPS in the TB-1 for the 731-g, Plutonium Metal Hollow Cylinder, Far Side Position, Side Impact (Range Adjusted to Highlight Small Stains in the TB-1 Not Visible in Figure 2-201) 2-175
Figure 2-203. Plot of von Mises Stress in the TB-1 for the 731-g, Plutonium Metal Hollow Cylinder, Far Side Position, Side Impact 2-175
Figure 2-204. Plot of von Mises Stress in the TB-1 for the 731-g, Plutonium Metal Hollow Cylinder, Far Side Position, Side Impact (see Figure 2-203 Rotated to Show Internal Stresses) 2-176
Figure 2-205. Finite Element Mesh for the 731-g, Angled, ER Cylinder, Far Side Position, Side Impact 2-177
Figure 2-206. Finite Element Mesh for the 731-g, Angled, ER Cylinder, Far Side Position, Side Impact – Final Displacement 2-177
Figure 2-207. Kinetic Energy Time History for the 731-g, Angled, Plutonium Metal Hollow Cylinder, Far Side Position, Side Impact 2-178

Figure 2-208. Graph of Average Stress Triaxiality versus EQPS of Elements Exceeding the Experimental Strain Locus for the 731-g, Angled, Plutonium Metal Hollow Cylinder, Far Side Position, Side Impact 2-178
Figure 2-209. Graph of Average Stress Triaxiality versus EQPS of Elements Exceeding the Experimental Strain Locus (Zoomed In) for the 731-g, Angled, Plutonium Metal Hollow Cylinder, Far Side Position, Side Impact 2-179
Figure 2-210. Graph of Tearing Parameter versus EQPS of Elements Exceeding the Experimental Strain Locus for the 731-g, Angled, Plutonium Metal Hollow Cylinder, Far Side Position, Side Impact 2-179
Figure 2-211. Plot of Elements Exceeding the Experimental Strain Locus for the 731-g, Angled, Plutonium Metal Hollow Cylinder, Far Side Position, Side Impact 2-180
Figure 2-212. Plot of EQPS in the TB-1 for the 731-g, Angled, Plutonium Metal Hollow Cylinder, Far Side Position, Side Impact 2-180
Figure 2-213. Plot of EQPS in the TB-1 for the 731-g, Angled, Plutonium Metal Hollow Cylinder, Far Side Position, Side Impact 2-181
Figure 2-214. Plot of von Mises Stress in the TB-1 for the 731-g, Angled, Plutonium Metal Hollow Cylinder, Far Side Position, Side Impact 2-181
Figure 2-215. Plot of von Mises Stress in the TB-1 for the 731-g, Angled, Plutonium Metal Hollow Cylinder, Far Side Position, Side Impact 2-182
Figure 2-216. Finite Element Mesh for the SC-1, Pu Contents, End Impact 2-184
Figure 2-217. Finite Element Mesh for the SC-1, Pu Contents, End Impact – Final Displacement 2-184
Figure 2-218. Kinetic Energy Time History for the SC-1, Pu Contents, End Impact 2-185
Figure 2-219. Plot of EQPS in the TB-1 for the SC-1, Pu Contents, End Impact 2-185
Figure 2-220. Plot of von Mises Stress in the TB-1 for the SC-1, Pu Contents, End Impact 2-186
Figure 2-221. Plot of Contact Force in the TB-1 for the SC-1, Pu Contents, End Impact 2-186
Figure 2-222. Finite Element Mesh for the SC-1, Pu Contents, Side Impact, 0° Support Structure 2-187
Figure 2-223. Finite Element Mesh for the SC-1, Pu Contents, Side Impact, 0° Support Structure – Final Displacement 2-188
Figure 2-224. Kinetic Energy Time History for the SC-1, Pu Contents, Side Impact, 0° Support Structure 2-188
Figure 2-225. Graph of Average Stress Triaxiality versus EQPS of Elements Exceeding the Experimental Strain Locus for the SC-1, Pu Contents, Side Impact, 0° Support Structure 2-189
Figure 2-226. Graph of Tearing Parameter versus EQPS of Elements Exceeding the Experimental Strain Locus for the SC-1, Pu Contents, Side Impact, 0° Support Structure 2-189
Figure 2-227. Plot of Elements Exceeding the Experimental Strain Locus for the SC-1, Pu Contents, Side Impact, 0° Support Structure 2-190
Figure 2-228. Plot of Elements Exceeding the Experimental Strain Locus for the SC-1, Pu Contents, Side Impact, 0° Support Structure 2-190
Figure 2-229. Plot of Elements Exceeding the Experimental Strain Locus for the SC-1, Pu Contents, Side Impact, 0° Support Structure 2-191

Figure 2-230. Plot of EQPS in the TB-1 for the SC-1, Pu Contents, Side Impact, 0° Support Structure 2-191
Figure 2-231. Plot of EQPS in the TB-1 for the SC-1, Pu Contents, Side Impact, 0° Support Structure 2-192
Figure 2-232. Plot of EQPS in the TB-1 for the SC-1, Pu Contents, Side Impact, 0° Support Structure 2-192
Figure 2-233. Plot of EQPS in the TB-1 for the SC-1, Pu Contents, Side Impact, 0° Support Structure 2-193
Figure 2-234. Plot of von Mises Stress in the TB-1 for the SC-1, Pu Contents, Side Impact, 0° Support Structure 2-193
Figure 2-235. Finite Element Mesh for the SC-1, Pu Contents, Side Impact, 45° Support Structure 2-194
Figure 2-236. Finite Element Mesh for the SC-1, Pu Contents, Side Impact, 45° Support Structure – Final Displacement 2-195
Figure 2-237. Kinetic Energy Time History for the SC-1, Pu Contents, Side Impact, 45° Support Structure 2-195
Figure 2-238. Graph of Average Stress Triaxiality versus EQPS of Elements Exceeding the Experimental Strain Locus for the SC-1, Pu Contents, Side Impact, 45° Support Structure 2-196
Figure 2-239. Graph of Tearing Parameter versus EQPS of Elements Exceeding the Experimental Strain Locus for the SC-1, Pu Contents, Side Impact, 45° Support Structure 2-196
Figure 2-240. Plot of Elements Exceeding the Experimental Strain Locus for the SC-1, Pu Contents, Side Impact, 45° Support Structure 2-197
Figure 2-241. Plot of Elements Exceeding the Experimental Strain Locus for the SC-1, Pu Contents, Side Impact, 45° Support Structure 2-197
Figure 2-242. Plot of EQPS in the TB-1 for the SC-1, Pu Contents, Side Impact, 45° Support Structure 2-198
Figure 2-243. Plot of EQPS in the TB-1 for the SC-1, Pu Contents, Side Impact, 45° Support Structure 2-198
Figure 2-244. Plot of EQPS in the TB-1 for the SC-1, Pu Contents, Side Impact, 45° Support Structure 2-199
Figure 2-245. Plot of EQPS in the TB-1 for the SC-1, Pu Contents, Side Impact, 45° Support Structure 2-199
Figure 2-246. Plot of von Mises Stress in the TB-1 for the SC-1, Pu Contents, Side Impact, 45° Support Structure 2-200
Figure 2-247. Finite Element Mesh for the SC-1, Pu Contents, CGOC Impact, 0° Support Structure 2-201
Figure 2-248. Finite Element Mesh for the SC-1, Pu Contents, CGOC Impact, 0° Support Structure – Final Displacement 2-201
Figure 2-249. Kinetic Energy Time History for the SC-1, Pu Contents, CGOC Impact, 0° Support Structure 2-202
Figure 2-250. Plot of EQPS in the TB-1 for the SC-1, Pu Contents, CGOC Impact, 0° Support Structure 2-202
Figure 2-251. Plot of EQPS in the TB-1 for the SC-1, Pu Contents, CGOC Impact, 0° Support Structure 2-203

Figure 2-252. Plot of von Mises Stress in the TB-1 for the SC-1, Pu Contents, CGOC Impact, 0° Support Structure 2-203
Figure 2-253. Plot of Contact Force in the TB-1 for the SC-1, Pu Contents, CGOC Impact, 0° Support Structure 2-204
Figure 2-254. Finite Element Mesh for the SC-1, Pu Contents, CGOC Impact, 45° Support Structure 2-205
Figure 2-255. Finite Element Mesh for the SC-1, Pu Contents, CGOC Impact, 45° Support Structure – Final Displacement 2-205
Figure 2-256. Kinetic Energy Time History for the SC-1, Pu Contents, CGOC Impact, 45° Support Structure 2-206
Figure 2-257. Plot of EQPS in the TB-1 for the SC-1, Pu Contents, CGOC Impact, 45° Support Structure 2-206
Figure 2-258. Plot of EQPS in the TB-1 for the SC-1, Pu Contents, CGOC Impact, 45° Support Structure 2-207
Figure 2-259. Plot of von Mises Stress in the TB-1 for the SC-1, Pu Contents, CGOC Impact, 45° Support Structure 2-207
Figure 2-260. Plot of Contact Forces in the TB-1 for the SC-1, Pu Contents, CGOC Impact, 45° Support Structure 2-208
Figure 2-261. Finite Element Mesh for the SC-2, End Impact, 0° Support Structure 2-209
Figure 2-262. Finite Element Mesh for the SC-2, End Impact, 0° Support Structure – Final Displacement 2-209
Figure 2-263. Kinetic Energy Time History for the SC-2, End Impact, 0° Support Structure 2-210
Figure 2-264. Plot of EQPS in the TB-1 for the SC-2, End Impact, 0° Support Structure 2-210
Figure 2-265. Plot of von Mises Stress in the TB-1 for the SC-2, End Impact, 0° Support Structure 2-211
Figure 2-266. Plot of Contact Forces in the TB-1 for the SC-2, End Impact, 0° Support Structure 2-211
Figure 2-267. Finite Element Mesh for the SC-2, Side Impact, 0° Support Structure 2-212
Figure 2-268. Finite Element Mesh for the SC-2, Side Impact, 0° Support Structure – Final Displacement 2-213
Figure 2-269. Kinetic Energy Time History for the SC-2, Side Impact, 0° Support Structure 2-213
Figure 2-270. Graph of Average Stress Triaxiality versus EQPS of Elements Exceeding the Experimental Strain Locus for the SC-2, Side Impact, 0° Support Structure 2-214
Figure 2-271. Graph of Tearing Parameter versus EQPS of Elements Exceeding the Experimental Strain Locus for the SC-2, Side Impact, 0° Support Structure 2-214
Figure 2-272. Plot of Elements Exceeding the Experimental Strain Locus for the SC-2, Side Impact, 0° Support Structure 2-215
Figure 2-273. Plot of Elements Exceeding the Experimental Strain Locus for the SC-2, Side Impact, 0° Support Structure 2-215
Figure 2-274. Plot of EQPS in the TB-1 for the SC-2, Side Impact, 0° Support Structure ... 2-216
Figure 2-275. Plot of EQPS in the TB-1 for the SC-2, Side Impact, 0° Support Structure ... 2-216

Figure 2-276. Plot of von Mises Stress in the TB-1 for the SC-2, Side Impact, 0° Support Structure 2-217
Figure 2-277. Finite Element Mesh for the SC-2, Side Impact, 45° Support Structure 2-218
Figure 2-278. Finite Element Mesh for the SC-2, Side Impact, 45° Support Structure – Final Displacement 2-218
Figure 2-279. Kinetic Energy Time History for the SC-2, Side Impact, 45° Support Structure 2-219
Figure 2-280. Graph of Average Stress Triaxiality versus EQPS of Elements Exceeding the Experimental Strain Locus for the SC-2, Side Impact, 45° Support Structure 2-219
Figure 2-281. Graph of Tearing Parameter versus EQPS of Elements Exceeding the Experimental Strain Locus for the SC-2, Side Impact, 45° Support Structure 2-220
Figure 2-282. Plot of Elements Exceeding the Experimental Strain Locus for the SC-2, Side Impact, 45° Support Structure 2-221
Figure 2-283. Plot of Elements Exceeding the Experimental Strain Locus for the SC-2, Side Impact, 45° Support Structure 2-222
Figure 2-284. Plot of EQPS in the TB-1 for the SC-2, Side Impact, 45° Support Structure 2-222
Figure 2-285. Plot of EQPS in the TB-1 for the SC-2, Side Impact, 45° Support Structure 2-223
Figure 2-286. Plot of EQPS in the TB-1 for the SC-2, Side Impact, 45° Support Structure 2-223
Figure 2-287. Plot of von Mises Stress in the TB-1 for the SC-2, Side Impact, 45° Support Structure 2-224
Figure 2-288. Finite Element Mesh for the SC-2, CGOC Impact, 0° Support Structure 2-225
Figure 2-289. Finite Element Mesh for the SC-2, CGOC Impact, 0° Support Structure – Final Displacement 2-225
Figure 2-290. Kinetic Energy Time History for the SC-2, CGOC Impact, 0° Support Structure 2-226
Figure 2-291. Plot of EQPS in the TB-1 for the SC-2, CGOC Impact, 0° Support Structure 2-226
Figure 2-292. Plot of von Mises Stress in the TB-1 for the SC-2, CGOC Impact, 0° Support Structure 2-227
Figure 2-293. Plot of Contact Forces in the TB-1 for the SC-2, CGOC Impact, 0° Support Structure 2-227
Figure 2-294. Finite Element Mesh for the SC-2, CGOC Impact, 45° Support Structure 2-228
Figure 2-295. Finite Element Mesh for the SC-2, CGOC Impact, 45° Support Structure – Final Displacement 2-229
Figure 2-296. Kinetic Energy Time History for the SC-2, CGOC Impact, 45° Support Structure 2-229
Figure 2-297. Plot of EQPS in the TB-1 for the SC-2, CGOC Impact, 45° Support Structure 2-230
Figure 2-298. Plot of von Mises Stress in the TB-1 for the SC-2, CGOC Impact, 45° Support Structure 2-230

Figure 2-299. Plot of Contact Forces in the TB-1 for the SC-2, CGOC Impact, 45° Support Structure 2-231
Figure 2-300. Finite Element Mesh for the SC-1, End Impact, 0° Support Structure, Be Contents 2-232
Figure 2-301. Finite Element Mesh for the SC-1, End Impact, 0° Support Structure, Be Contents – Final Displacement 2-232
Figure 2-302. Kinetic Energy Time History for the SC-1, End Impact, 0° Support Structure, Be Contents 2-233
Figure 2-303. Plot of EQPS in the TB-1 for the SC-1, End Impact, 0° Support Structure, Be Contents 2-233
Figure 2-304. Plot of von Mises Stress in the TB-1 for the SC-1, End Impact, 0° Support Structure, Be Contents 2-234
Figure 2-305. Finite Element Mesh for the SC-1, Side Impact, 0° Support Structure, Be Contents 2-235
Figure 2-306. Finite Element Mesh for the SC-1, Side Impact, 0° Support Structure, Be Contents – Final Displacement 2-235
Figure 2-307. Kinetic Energy Time History for the SC-1, Side Impact, 0° Support Structure, Be Contents 2-236
Figure 2-308. Graph of Average Stress Triaxiality versus EQPS of the Elements Exceeding the Experimental Strain Locus for the SC-1, Side Impact, 0° Support Structure, Be Contents 2-236
Figure 2-309. Graph of Average Stress Triaxiality versus EQPS of the Elements Exceeding the Experimental Strain Locus (Zoomed In) for the SC-1, Side Impact, 0° Support Structure, Be Contents 2-237
Figure 2-310. Graph of Tearing Parameter versus EQPS of the Elements Exceeding the Experimental Strain Locus for the SC-1, Side Impact, 0° Support Structure, Be Contents 2-237
Figure 2-311. Plot of the Elements Exceeding the Experimental Strain Locus for the SC-1, Side Impact, 0° Support Structure, Be Contents 2-238
Figure 2-312. Plot of the Elements Exceeding the Experimental Strain Locus for the SC-1, Side Impact, 0° Support Structure, Be Contents 2-238
Figure 2-313. Plot of EQPS in the TB-1 for the SC-1, Side Impact, 0° Support Structure, Be Contents 2-239
Figure 2-314. Plot of von Mises Stress in the TB-1 for the SC-1, Side Impact, 0° Support Structure, Be Contents 2-239
Figure 2-315. Finite Element Mesh for the SC-1, Side Impact, 45° Support Structure, Be Contents 2-240
Figure 2-316. Finite Element Mesh for the SC-1, Side Impact, 45° Support Structure, Be Contents – Final Displacement 2-241
Figure 2-317. Kinetic Energy Time History for the SC-1, Side Impact, 45° Support Structure, Be Contents 2-241
Figure 2-318. Graph of Average Stress Triaxiality versus EQPS of Elements Exceeding the Experimental Strain Locus for the SC-1, Side Impact, 45° Support Structure, Be Contents 2-242

Figure 2-319. Graph of Tearing Parameter versus EQPS of Elements Exceeding the Experimental Strain Locus for the SC-1, Side Impact, 45° Support Structure, Be Contents 2-242
Figure 2-320. Plot of Elements Exceeding the Experimental Strain Locus for the SC-1, Side Impact, 45° Support Structure, Be Contents 2-243
Figure 2-321. Plot of Elements Exceeding the Experimental Strain Locus for the SC-1, Side Impact, 45° Support Structure, Be Contents 2-243
Figure 2-322. Plot of EQPS in the TB-1 for the SC-1, Side Impact, 45° Support Structure, Be Contents 2-244
Figure 2-323. Plot of von Mises Stress in the TB-1 for the SC-1, Side Impact, 45° Support Structure, Be Contents 2-244
Figure 2-324. Finite Element Mesh for the SC-1, CGOC Impact, 0° Support Structure, Be Contents 2-245
Figure 2-325. Finite Element Mesh for the SC-1, CGOC Impact, 0° Support Structure, Be Contents – Final Displacement 2-246
Figure 2-326. Kinetic Energy Time History for the SC-1, CGOC Impact, 0° Support Structure, Be Contents 2-246
Figure 2-327. Plot of EQPS in the TB-1 for the SC-1, CGOC Impact, 0° Support Structure, Be Contents 2-247
Figure 2-328. Plot of von Mises Stress in the TB-1 for the SC-1, CGOC Impact, 0° Support Structure, Be Contents 2-247
Figure 2-329. Finite Element Mesh for the SC-1, CGOC Impact, 45° Support Structure, Be Contents 2-248
Figure 2-330. Finite Element Mesh for the SC-1, CGOC Impact, 45° Support Structure, Be Contents – Final Displacement 2-249
Figure 2-331. Kinetic Energy Time History for the SC-1, CGOC Impact, 45° Support Structure, Be Contents 2-249
Figure 2-332. Plot of EQPS in the TB-1 for the SC-1, CGOC Impact, 45° Support Structure, Be Contents 2-250
Figure 2-333. Plot of EQPS in the TB-1 for the SC-1, CGOC Impact, 45° Support Structure, Be Contents 2-250
Figure 2-334. Plot of von Mises Stress in the TB-1 for the SC-1, CGOC Impact, 45° Support Structure, Be Contents 2-251
Figure 2-335. Finite Element Mesh for the SC-2, Side Impact, 45° Support Structure, Friction 0.4 2-252
Figure 2-336. Finite Element Mesh for the SC-2, Side Impact, 45° Support Structure, Friction 0.4 – Final Displacement 2-253
Figure 2-337. Kinetic Energy Time History for the SC-2, Side Impact, 45° Support Structure, Friction 0.4 2-253
Figure 2-338. Graph of Average Stress Triaxiality versus EQPS of Elements Exceeding the Experimental Strain Locus for the SC-2, Side Impact, 45° Support Structure, Friction 0.4 2-254
Figure 2-339. Graph of Tearing Parameter versus EQPS of Elements Exceeding the Experimental Strain Locus for the SC-2, Side Impact, 45° Support Structure, Friction 0.4 2-254

Figure 2-340. Plot of Elements Exceeding the Experimental Strain Locus for the SC-2, Side Impact, 45° Support Structure, Friction 0.4 2-255
Figure 2-341. Plot of Elements Exceeding the Experimental Strain Locus for the SC-2, Side Impact, 45° Support Structure, Friction 0.4 2-255
Figure 2-342. Plot of Elements Exceeding the Experimental Strain Locus for the SC-2, Side Impact, 45° Support Structure, Friction 0.4 2-256
Figure 2-343. Plot of EQPS in the TB-1 for the SC-2, Side Impact, 45° Support Structure, Friction 0.4 2-256
Figure 2-344. Plot of EQPS in the TB-1 for the SC-2, Side Impact, 45° Support Structure, Friction 0.4 2-257
Figure 2-345. Plot of von Mises Stress in the TB-1 for the SC-2, Side Impact, 45° Support Structure, Friction 0.4 2-257
Figure 2-346. Finite Element Mesh for the SC-2, Side Impact, 45° Support Structure, Friction 0.2 2-259
Figure 2-347. Finite Element Mesh for the SC-2, Side Impact, 45° Support Structure, Friction 0.2 – Final Displacement 2-259
Figure 2-348. Kinetic Energy Time History for the SC-2, Side Impact, 45° Support Structure, Friction 0.2 2-260
Figure 2-349. Graph of Average Stress Triaxiality versus EQPS of Elements Exceeding the Experimental Strain Locus for the SC-2, Side Impact, 45° Support Structure, Friction 0.2 2-260
Figure 2-350. Graph of Tearing Parameter versus EQPS of Elements Exceeding the Experimental Strain Locus for the SC-2, Side Impact, 45° Support Structure, Friction 0.2 2-261
Figure 2-351. Plot of Elements Exceeding the Experimental Strain Locus for the SC-2, Side Impact, 45° Support Structure, Friction 0.2 2-261
Figure 2-352. Plot of Elements Exceeding the Experimental Strain Locus for the SC-2, Side Impact, 45° Support Structure, Friction 0.2 2-262
Figure 2-353. Plot of EQPS in the TB-1 for the SC-2, Side Impact, 45° Support Structure, Friction 0.2 2-262
Figure 2-354. Plot of EQPS in the TB-1 for the SC-2, Side Impact, 45° Support Structure, Friction 0.2 2-263
Figure 2-355. Plot of von Mises Stress in the TB-1 for the SC-2, Side Impact, 45° Support Structure, Friction 0.2 2-263
Figure 2-356. Summary Plot of Lid Retaining Forces and Component Impulse Loads 2-267
Figure 2-357. Summary Plot of Plastic Stress Triaxiality for Selected Runs 2-267
Figure 2-358. Finite Element Mesh for HAC Run 1, SC-2, End Impact 2-270
Figure 2-359. Finite Element Mesh for HAC Run 1, SC-2, End Impact – Final Displacement 2-271
Figure 2-360. Kinetic Energy Time History for HAC Run 1, SC-2, End Impact 2-271
Figure 2-361. Tresca Stress in TB-1 for HAC Run 1, SC-2, End Impact 2-272
Figure 2-362. Tresca Stress of TB-1 for HAC Run 1, SC-2, End Impact 2-272
Figure 2-363. Tresca Stress of TB-1 for HAC Run 1, SC-2, End Impact when Plate Velocity Reaches Zero 2-273
Figure 2-364. Finite Element Mesh for HAC Run 2, SC-2, Side Impact, Support Structure 0° 2-274

Figure 2-365. Finite Element Mesh for HAC Run 2, SC-2, Side Impact, Support Structure 0° - Final Displacement 2-274
Figure 2-366. Kinetic Energy Time History for HAC Run 2, SC-2, Side Impact, Support Structure 0° 2-275
Figure 2-367. Graph of Average Stress Triaxiality versus EQPS for Element Exceeding Experimental Strain Locus for HAC Run 2, SC-2, Side Impact, Support Structure 0° 2-275
Figure 2-368. Graph of Average Stress Triaxiality versus EQPS for Element Exceeding Experimental Strain Locus (Zoomed In) for HAC Run 2, SC-2, Side Impact, Support Structure 0° 2-276
Figure 2-369. Graph of Tearing Parameter versus EQPS for Element Exceeding Experimental Strain Locus for HAC Run 2, SC-2, Side Impact, Support Structure 0° 2-276
Figure 2-370. Plot of Element Exceeding Experimental Strain Locus for HAC Run 2, SC 2, Side Impact, Support Structure 0° 2-277
Figure 2-371. Graph of EQPS in the TB-1 for HAC Run 2, SC-2, Side Impact, Support Structure 0° 2-277
Figure 2-372. Plot of Tresca Stress in the TB-1 for HAC Run 2, SC-2, Side Impact, Support Structure 0° 2-278
Figure 2-373. Plot of Tresca Stress in the TB-1 for HAC Run 2, SC-2, Side Impact, Support Structure 0° when Plate Velocity Reaches Zero 2-278
Figure 2-374. Finite Element Mesh for HAC Run 3, SC-2, Side Impact, Support Structure 45° 2-279
Figure 2-375. Finite Element Mesh for HAC Run 3, SC-2, Side Impact, Support Structure 45° - Final Displacement 2-280
Figure 2-376. Kinetic Energy Time History for HAC Run 3, SC-2, Side Impact, Support Structure 45° 2-280
Figure 2-377. Graph of Average Stress Triaxiality versus EQPS of Element Exceeding Experimental Strain Locus for HAC Run 3, SC-2, Side Impact, Support Structure 45° 2-281
Figure 2-378. Graph of Tearing Parameter versus EQPS of Element Exceeding Experimental Strain Locus (Zoomed In) for HAC Run 3, SC-2, Side Impact, Support Structure 45° 2-281
Figure 2-379. Plot of Element Exceeding Experimental Strain Locus for HAC Run 3, SC 2, Side Impact, Support Structure 45° 2-282
Figure 2-380. Plot of EQPS in the TB-1 for HAC Run 3, SC-2, Side Impact, Support Structure 45° 2-282
Figure 2-381. Plot of Tresca Stress in the TB-1 for HAC Run 3, SC-2, Side Impact, Support Structure 45° 2-283
Figure 2-382. Plot of Tresca Stress in the TB-1 for HAC Run 3, SC-2, Side Impact, Support Structure 45° 2-283
Figure 2-383. Plot of Tresca Stress in the TB-1 for HAC Run 3, SC-2, Side Impact, Support Structure 45° when Plate Velocity Reaches Zero 2-284
Figure 2-384. Finite Element Mesh for HAC Run 4, SC-2, CGOC Impact, Support Structure 0° 2-285

Figure 2-385. Finite Element Mesh for HAC Run 4, SC-2, CGOC Impact, Support Structure 0°, Final Displacement 2-285
Figure 2-386. Kinetic Energy Time History for HAC Run 4, SC-2, CGOC Impact, Support Structure 0° 2-286
Figure 2-387. Plot of EQPS in TB-1 for HAC Run 4, SC-2, CGOC Impact, Support Structure 0° 2-286
Figure 2-388. Plot of Tresca Stress in TB-1 for HAC Run 4, SC-2, CGOC Impact, Support Structure 0° 2-287
Figure 2-389. Plot of Tresca Stress in the TB-1 for HAC Run 4, SC-2, CGOC Impact, Support Structure 0° when Plate Velocity Reaches Zero 2-287
Figure 2-390. Finite Element Mesh for HAC Run 5, SC-2, CGOC Impact, Support Structure 45° 2-288
Figure 2-391. Finite Element Mesh for HAC Run 5, SC-2, CGOC Impact, Support Structure 45° - Final Displacement 2-289
Figure 2-392. Kinetic Energy Time History for HAC Run 5, SC-2, CGOC Impact, Support Structure 45° 2-289
Figure 2-393. Plot of Tresca Stress in the TB-1 for HAC Run 5, SC-2, CGOC Impact, Support Structure 45° when Stress is a Maximum 2-290
Figure 2-394. Finite Element Mesh for HAC Run 6, SC-1, End Impact, Support Structure 0° 2-291
Figure 2-395. Finite Element Mesh for HAC Run 6, SC-1, End Impact, Support Structure 0° - Final Displacement 2-291
Figure 2-396. Kinetic Energy Time History for HAC Run 6, SC-1, End Impact, Support Structure 0° 2-292
Figure 2-397. Plot of Tesca Stress in the TB-1 for HAC Run 6, SC-1, End Impact, Support Structure 0° 2-292
Figure 2-398. Plot of Tresca Stress in the TB-1 for HAC Run 6, SC-1, End Impact, Support Structure 0° when Plate Velocity Reaches Zero 2-293
Figure 2-399. Finite Element Mesh for HAC Run 7, SC-1, Side Impact, Support Structure 0° 2-294
Figure 2-400. Finite Element Mesh for HAC Run 7, SC-1, Side Impact, Support Structure 0° - Final Displacement 2-294
Figure 2-401. Kinetic Energy Time History for HAC Run 7, SC-1, Side Impact, Support Structure 0° 2-295
Figure 2-402. Plot of EQPS in TB-1 for HAC Run 7, SC-1, Side Impact, Support Structure 0° 2-295
Figure 2-403. Plot of Tresca Stress in the TB-1 for HAC Run 7, SC-1, Side Impact, Support Structure 0° 2-296
Figure 2-404. Plot of Tresca Stress in the TB-1 for HAC Run 7, SC-1, Side Impact, Support Structure 0° when Plate Velocity Reaches Zero 2-296
Figure 2-405. Finite Element Mesh for HAC Run 8, SC-1, Side Impact, Support Structure 45° 2-297
Figure 2-406. Finite Element Mesh for HAC Run 8, SC-1, Side Impact, Support Structure 45° - Final Displacement 2-298
Figure 2-407. Kinetic Energy Time History for HAC Run 8, SC-1, Side Impact, Support Structure 45° 2-298

Figure 2-408. Plot of EQPS in TB-1 for HAC Run 8, SC-1, Side Impact, Support Structure 45° 2-299
Figure 2-409. Plot of Tresca Stress in TB-1 for HAC Run 8, SC-1, Side Impact, Support Structure 45° 2-299
Figure 2-410. Plot of Tresca Stress in TB-1 for HAC Run 8, SC-1, Side Impact, Support Structure 45° 2-300
Figure 2-411. Plot of Tresca Stress in TB-1 for HAC Run 8, SC-1, Side Impact, Support Structure 45° when Plate Velocity Reaches Zero 2-300
Figure 2-412. Finite Element Mesh for HAC Run 9, SC-1, CGOC Impact, Support Structure 0° 2-301
Figure 2-413. Finite Element Mesh for HAC Run 9, SC-1, CGOC Impact, Support Structure 0° - Final Displacement 2-302
Figure 2-414. Kinetic Energy Time History for HAC Run 9, SC-1, CGOC Impact, Support Structure 0° 2-302
Figure 2-415. Tresca Stress for HAC Run 9, SC-1, CGOC Impact, Support Structure 0° 2-303
Figure 2-416. Plot of Tresca Stress in the TB-1 for HAC Run 9, SC-1, CGOC Impact, Support Structure 0° when Plate Velocity Reaches Zero 2-303
Figure 2-417. Finite Element Mesh for HAC Run 10, SC-1, CGOC Impact, Support Structure 45° 2-304
Figure 2-418. Finite Element Mesh for HAC Run 10, SC-1, CGOC Impact, Support Structure 45° - Final Displacement 2-305
Figure 2-419. Kinetic Energy Time History for HAC Run 10, SC-1, CGOC Impact, Support Structure 45° 2-305
Figure 2-420. Plot of Tresca Stress in the TB-1 for HAC Run 10, SC-1, CGOC Impact, Support Structure 45° 2-306
Figure 2-421. Plot of Tresca Stress in the TB-1 for HAC Run 10, SC-1, CGOC Impact, Support Structure 45° when Plate Velocity Reaches Zero 2-306
Figure 2-422. Finite Element Mesh for HAC Run 11, 831 g Plutonium Metal Hollow Cylinder, End Impact 2-307
Figure 2-423. Finite Element Mesh for HAC Run 11, 831 g, Plutonium Metal Hollow Cylinder, End Impact – Final Displacement 2-308
Figure 2-424. Kinetic Energy Time History for HAC Run 11, 831 g, Plutonium Metal Hollow Cylinder, End Impact 2-308
Figure 2-425. Plot of EQPS in the TB-1 for HAC Run 11, 831 g, Plutonium Metal Hollow Cylinder, End Impact 2-309
Figure 2-426. Plot of Tresca Stress in the TB-1 for HAC Run 11, 831 g, Plutonium Metal Hollow Cylinder, End Impact 2-309
Figure 2-427. Plot of Tresca Stress in the TB-1 for HAC Run 11, 831 g Plutonium Metal Hollow Cylinder, End Impact when Plate Velocity Reaches Zero 2-310
Figure 2-428. Finite Element Mesh for HAC Run 12, 831 g, Plutonium Metal Hollow Cylinder, Side Impact 2-311
Figure 2-429. Finite Element Mesh for HAC Run 12, 831 g, Plutonium Metal Hollow Cylinder, Side Impact – Final Displacement 2-311
Figure 2-430. Kinetic Energy Time History for HAC Run 12, 831 g, Plutonium Metal Hollow Cylinder, Side Impact 2-312

Figure 2-431. Plot of EQPS in the TB-1 for HAC Run 12, 831 g, Plutonium Metal Hollow Cylinder, Side Impact 2-312
Figure 2-432. Plot of Tresca Stress in the TB-1 for HAC Run 12, 831 g Plutonium Metal Hollow Cylinder, Side Impact 2-313
Figure 2-433. Plot of Tresca Stress for HAC Run 12, 831 g Plutonium Metal Hollow Cylinder, Side Impact 2-313
Figure 2-434. Plot of Tresca Stress for HAC Run 12, 831 g Plutonium Metal Hollow Cylinder, Side Impact when Plate Velocity Reaches Zero 2-314
Figure 2-435. Finite Element Mesh for HAC Run 13, 831 g, Angled, Plutonium Metal Hollow Cylinder, End Impact 2-315
Figure 2-436. Finite Element Mesh for HAC Run 13, 831 g, Angled, Plutonium Metal Hollow Cylinder, End Impact – Final Displacement 2-315
Figure 2-437. Kinetic Energy Time History for HAC Run 13, 831 g, Angled, Plutonium Metal Hollow Cylinder, End Impact 2-316
Figure 2-438. Plot of EQPS in the TB-1 for HAC Run 13, 831 g, Angled, Plutonium Metal Hollow Cylinder, End Impact 2-316
Figure 2-439. Plot of Tresca Stress in the TB-1 for HAC Run 13, 831 g, Angled, Plutonium Metal Hollow Cylinder, End Impact 2-317
Figure 2-440. Plot of Tresca Stress in the TB-1 for HAC Run 13, 831 g Angled Plutonium Metal Hollow Cylinder, End Impact when Plate Velocity Reaches Zero 2-317
Figure 2-441. Finite Element Mesh for HAC Run 14, 831 g, Angled, Plutonium Metal Hollow Cylinder, Side Impact 2-318
Figure 2-442. Finite Element Mesh for HAC Run 14, 831 g, Angled, Plutonium Metal Hollow Cylinder, Side Impact – Final Displacement 2-319
Figure 2-443. Kinetic Energy Time History for HAC Run 14, 831 g Angled Plutonium Metal Hollow Cylinder, Side Impact 2-319
Figure 2-444. Plot of EQPS in the TB-1 for HAC Run 14, 831 g Angled Plutonium Metal Hollow Cylinder, Side Impact 2-320
Figure 2-445. Plot of Tresca Stress in the TB-1 for HAC Run 14, 831 g, Angled, Plutonium Metal Hollow Cylinder, Side Impact 2-320
Figure 2-446. Plot of Tresca Stress in the TB-1 for HAC Run 14, 831 g Angled Plutonium Metal Hollow Cylinder, Side Impact when Plate Velocity Reaches Zero 2-321
Figure 2-447. Finite Element Mesh for HAC Run 15, 831 g Angled Plutonium Metal Hollow Cylinder, CGOC Impact 2-322
Figure 2-448. Finite Element Mesh for HAC Run 15, 831 g, Angled Plutonium Metal Hollow Cylinder, CGOC Impact – Final Displacement 2-322
Figure 2-449. Kinetic Energy Time History for HAC Run 15, 831 g Angled Plutonium Metal Hollow Cylinder, CGOC Impact 2-323
Figure 2-450. Plot of Tresca Stress in the TB-1 for HAC Run 15, 831 g Angled Plutonium Metal Hollow Cylinder, CGOC Impact 2-323
Figure 2-451. Plot of Tresca Stress in the TB-1 for HAC Run 15, 831 g Angled Plutonium Metal Hollow Cylinder, CGOC Impact when Plate Velocity Reaches Zero .. 2-324
Figure 2-452. Finite Element Mesh for HAC Run 16, 731 g, Plutonium Metal Hollow Cylinder, End Impact 2-325
Figure 2-453. Finite Element Mesh for HAC Run 16, 731 g, Plutonium Metal Hollow Cylinder, End Impact – Final Displacement 2-325

Figure 2-454. Kinetic Energy Time History for HAC Run 16, 731 g, Plutonium Metal Hollow Cylinder, End Impact 2-326
Figure 2-455. Plot of EQPS in the TB-1 for HAC Run 16, 731 g, Plutonium Metal Hollow Cylinder, End Impact 2-326
Figure 2-456. Plot of EQPS in the TB-1 for HAC Run 16, 731 g, Plutonium Metal Hollow Cylinder, End Impact 2-327
Figure 2-457. Plot of Tresca Stress in the TB-1 for HAC Run 16, 731 g, Plutonium Metal Hollow Cylinder, End Impact 2-327
Figure 2-458. Plot of Tresca Stress in the TB-1 for HAC Run 16, 731 g Plutonium Metal Hollow Cylinder, End Impact when Plate Velocity Reaches Zero 2-328
Figure 2-459. Finite Element Mesh for HAC Run 17, 731 g, Plutonium Metal Hollow Cylinder, Side Impact 2-329
Figure 2-460. Finite Element Mesh for HAC Run 17, 731 g, Plutonium Metal Hollow Cylinder, Side Impact – Final Displacement 2-329
Figure 2-461. Kinetic Energy Time History for HAC Run 17, 731 g, Plutonium Metal Hollow Cylinder, Side Impact 2-330
Figure 2-462. Plot of EQPS in the TB-1 for HAC Run 17, 731 g, Plutonium Metal Hollow Cylinder, Side Impact 2-330
Figure 2-463. Plot of Tresca Stress in the TB-1 for HAC Run 17, 731 g, Plutonium Metal Hollow Cylinder, Side Impact 2-331
Figure 2-464. Plot of Tresca Stress in the TB-1 for HAC Run 17, 731 g, Plutonium Metal Hollow Cylinder, Side Impact 2-331
Figure 2-465. Plot of Tresca Stress in the TB-1 for HAC Run 17, 731 g Plutonium Metal Hollow Cylinder, Side Impact when Plate Velocity Reaches Zero 2-332
Figure 2-466. Finite Element Mesh for HAC Run 18, 731 g, Angled, Plutonium Metal Hollow Cylinder, End Impact 2-333
Figure 2-467. Finite Element Mesh for HAC Run 18, 731 g, Angled, Plutonium Metal Hollow Cylinder, End Impact – Final Displacement 2-333
Figure 2-468. Kinetic Energy Time History for HAC Run 18, 731 g, Angled, Plutonium Metal Hollow Cylinder, End Impact 2-334
Figure 2-469. Plot of EQPS in the TB-1 for HAC Run 18, 731 g, Angled, Plutonium Metal Hollow Cylinder, End Impact 2-334
Figure 2-470. Plot of Tresca Stress in the TB-1 for HAC Run 18, 731 g, Angled, Plutonium Metal Hollow Cylinder, End Impact 2-335
Figure 2-471. Plot of Tresca Stress in the TB-1 for HAC Run 18, 731 g, Angled, Plutonium Metal Hollow Cylinder, End Impact 2-335
Figure 2-472. Plot of Tresca Stress in the TB-1 for HAC Run 18, 731 g Angled Plutonium Metal Hollow Cylinder, End Impact when Plate Velocity Reaches Zero 2-336
Figure 2-473. Finite Element Mesh for HAC Run 19, 731 g, Angled, Plutonium Metal Hollow Cylinder, Side Impact 2-337
Figure 2-474. Finite Element Mesh for HAC Run 19, 731 g, Angled, Plutonium Metal Hollow Cylinder, Side Impact – Final Displacement 2-337
Figure 2-475. Kinetic Energy Time History for HAC Run 19, 731 g, Angled, Plutonium Metal Hollow Cylinder, Side Impact 2-338

Figure 2-476. Graph of Average Stress Triaxiality versus EQPS for Elements Exceeding the Experimental Strain Locus for HAC Run 19, 731 g, Angled, Plutonium Metal Hollow Cylinder, Side Impact 2-338
Figure 2-477. Graph of Average Stress Triaxiality versus EQPS for Elements Exceeding the Experimental Strain Locus (Zoomed In) for HAC Run 19, 731 g, Angled, Plutonium Metal Hollow Cylinder, Side Impact 2-339
Figure 2-478. Graph of Tearing Parameter versus EQPS for Elements Exceeding the Experimental Strain Locus for HAC Run 19, 731 g, Angled, Plutonium Metal Hollow Cylinder, Side Impact 2-339
Figure 2-479. Plot of Elements Exceeding the Experimental Strain Locus for HAC Run 19, 731 g, Angled, Plutonium Metal Hollow Cylinder, Side Impact 2-340
Figure 2-480. Plot of EQPS in the TB-1 for HAC Run 19, 731 g, Angled, Plutonium Metal Hollow Cylinder, Side Impact 2-340
Figure 2-481. Plot of Tresca Stress in the TB-1 for HAC Run 19, 731 g, Angled, Plutonium Metal Hollow Cylinder, Side Impact 2-341
Figure 2-482. Plot of Tresca Stress in the TB-1 for HAC Run 19, 731 g, Angled, Plutonium Metal Hollow Cylinder, Side Impact 2-341
Figure 2-483. Plot of Tresca Stress in the TB-1 for HAC Run 19, 731 g Angled Plutonium Metal Hollow Cylinder, Side Impact when Plate Velocity Reaches Zero 2-342
Figure 2-484. Finite Element Mesh for HAC Run 20, 731 g, Angled, Plutonium Metal Hollow Cylinder, CGOC Impact 2-343
Figure 2-485. Finite Element Mesh for HAC Run 20, 731 g, Angled, Plutonium Metal Hollow Cylinder, CGOC Impact – Final Displacement 2-343
Figure 2-486. Kinetic Energy Time History for HAC Run 20, 731 g, Angled, Plutonium Metal Hollow Cylinder, CGOC Impact 2-344
Figure 2-487. Plot of EQPS in the TB-1 for HAC Run 20, 731 g, Angled, Plutonium Metal Hollow Cylinder, CGOC Impact 2-344
Figure 2-488. Plot of Tresca Stress in the TB-1 for HAC Run 20, 731 g, Angled, Plutonium Metal Hollow Cylinder, CGOC Impact 2-345
Figure 2-489. Plot of Tresca Stress in the TB-1 for HAC Run 20, 731 g Angled Plutonium Metal Hollow Cylinder, CGOC Impact when Plate Velocity Reaches Zero .. 2-345
Figure 2-490. Finite Element Mesh for 30-ft Drop Run 1 – SC-2 with Support Structure Rotated 45 Degrees and Side Impact 2-346
Figure 2-491. Final Displacement in Finite Element Mesh for 30-ft Drop Run 1 – SC-2 with Support Structure Rotated 45 Degrees and Side Impact 2-347
Figure 2-492. Final Displacement in SAR1 Test for 30-ft Drop 2-347
Figure 2-493. Kinetic Energy for 30-ft Drop Run 1 – SC-2 with Support Structure Rotated 45 Degrees and Side Impact 2-348
Figure 2-494. EQPS in the T-Amp for 30-ft Drop Run 1 – SC-2 with Support Structure Rotated 45 Degrees and Side Impact 2-348
Figure 2-495. Tresca Stress in the TB-1 for 30-ft Drop Run 1 – SC-2 with Support Structure Rotated 45 Degrees and Side Impact 2-349
Figure 2-496. Finite Element Mesh for 30-ft Drop Run 2 – Angled 831 g Plutonium Metal Hollow Cylinder with End Impact 2-350
Figure 2-497. Final Displacement for 30-ft Drop Run 2 – Angled 831 g Plutonium Metal Hollow Cylinder with End Impact 2-350

Figure 2-498. Kinetic Energy for 30-ft Drop Run 2 – Angled 831 g Plutonium Metal Hollow Cylinder with End Impact 2-351
Figure 2-499. EQPS in TB-1 for 30-ft Drop Run 2 – Angled 831 g Plutonium Metal Hollow Cylinder with End Impact 2-351
Figure 2-500. Tresca Stress in the TB-1 for 30-ft Drop Run 2 – Angled 831 g Plutonium Metal Hollow Cylinder with End Impact 2-352
Figure 2-501. Finite Element Mesh for 30-ft Drop Run 3 – Angled 831 g Plutonium Metal Hollow Cylinder with CGOC Impact 2-353
Figure 2-502. Final Displacement for 30-ft Drop Run 3 – Angled 831 g Plutonium Metal Hollow Cylinder with CGOC Impact 2-353
Figure 2-503. Kinetic Energy for 30-ft Drop Run 3 – Angled 831 g Plutonium Metal Hollow Cylinder with CGOC Impact 2-354
Figure 2-504. Tresca Stress in the TB-1 for 30-ft Drop Run 3 – Angled 831 g Plutonium Metal Hollow Cylinder with CGOC Impact 2-354
Figure 2-505. Contact Forces on the Top Surface of the TB-1 Lid 2-356
Figure 2-506. Contact Forces on the Top Surface of the TB-1 Lid Along with Impulse Loads from Various Contents 2-357

Figure 3-1. Schematic of Assumed Worst-Case Heating-to-the-Seal Scenario 3-3
Figure 3-2. Schematic of Approximated Projected Heating Area [m=0.0254*in.; m^2=6.45x10-4*$in.^2$] 3-3
Figure 3-3. Finite Element Mesh of the PAT-1 Half-Symmetry Thermal Model and Enlarged Load Spreader, Copper Cylinder, TB-1, and T-Ampoule 3-9
Figure 3-4. Low-Temperature Thermal Test Simulation Results. (°C=[°F-32]/1.8) 3-11
Figure 3-5. Seven-day Thermal Cycling for Quasi-Steady-State Analysis – Package Mid Height Response (°C=[°F-32]/1.8) 3-12
Figure 3-6. NCT Daily Thermal Cycle (Quasi-Steady-State NCT Solution) – Package Mid Height Response (°C=[°F-32]/1.8) 3-12
Figure 3-7. Temperature Distribution of PAT-1 Just Before Sundown – Most Severe Case of Transient NCT SAR1 Analysis (Plot of ¼ of Package, °C=[°F-32]/1.8) 3-13
Figure 3-8. Temperature Distribution of PAT-1 – Steady-State NCT SAR1 Analysis (Plot of ¼ of Package, °C=[°F-32]/1.8) 3-13
Figure 3-9. NCT Steady-State Temperature Distribution (°C=[°F-32]/1.8) 3-14
Figure 3-10. Steady-State Analysis in the Shade – 10 CFR 71.43(g) (°C=[°F-32]/1.8) 3-15
Figure 3-11. Temperature Distribution of the Verification Model at the End of the 52 Minute Fire — Complete Model (°C=[°F-32]/1.8) 3-19
Figure 3-12. Temperature Distribution of the Verification Model at the End of the 52 Minute Fire — T-Ampoule, TB-1, Heat Transfer Cu Cylinder, and Aluminum Load Spreader (°C=[°F-32]/1.8) 3-19
Figure 3-13. Temperature Distribution of the Verification Model at t=352 Minutes (300 Minutes after the 52 Minute Fire) — Complete Model (°C=[°F-32]/1.8) 3-20
Figure 3-14. Temperature Distribution of the Verification Model at t=352 Minutes (300 Minutes after the 52 Minute Fire) — T-Ampoule, TB-1, Heat Transfer Cu Cylinder, and Aluminum Load Spreader (°C=[°F-32]/1.8) 3-20

Figure 3-15. Temperature History at T-Ampoule Seal Height for the 52-Minute Fire Model Verification Exercise (°C=[°F-32]/1.8). Note: In the schematic above the plot, the reference yellow line crosses the cask at the T-Ampoule-seal height and the white dots are the approximate locations of the temperature history lines in the plot. The "T-Ampoule (Seal)" curve is completely covered by the "TB-1" curve. 3-22
Figure 3-16. Temperature Distribution at the End of the 30 Minute Regulatory Fire — Complete Model (°C=[°F-32]/1.8) 3-23
Figure 3-17. Temperature Distribution at the End of the 30 Minute Regulatory Fire — T-Ampoule, TB-1, Heat Transfer Cu Cylinder, and Aluminum Load Spreader (°C=[°F-32]/1.8) 3-24
Figure 3-18. Temperature Distribution at t=290 Minutes (260 Minutes after the 30 Minute Fire) — Complete Model (°C=[°F-32]/1.8) 3-24
Figure 3-19. Temperature Distribution at t=290 Minutes (260 Minutes after the 30 Minute Fire) — T-Ampoule, TB-1, Heat Transfer Cu Cylinder, and Aluminum Load Spreader (°C=[°F-32]/1.8) 3-25
Figure 3-20. Temperature History at T-Ampoule Seal Height for the 30-Minute Regulatory Fire (°C=[°F-32]/1.8). Note: In the schematic above the plot, the reference yellow line crosses the cask at T-Ampoule-seal height and the white dots are the approximate locations of the temperature history lines in the plot. 3-26

Figure 4-1. TB-1 Containment Vessel and T-Ampoule Contents Container 4-2

Figure 5-1. Cylindrical Shielding Model of PAT-1 Used in This Analysis (see Table 5-6 for Dimensional Information) 5-7
Figure 5-2. Dose Locations Analyzed for the PAT-1 Package 5-11
Figure 5-3. Photon Source per Gram of Each Isotope of Pu Initially Present (Note That Pu-241 Data Includes Buildup of Am-241) 5-16
Figure 5-4. Neutron Source per Gram of Each Isotope of Pu Initially Present (Includes Both Spontaneous Fission and (α,n) Components with an Oxide Matrix; Also Note That Pu-241 Data Includes Buildup of Am-241) 5-17
Figure 5-5. Watts per Gram of Each Isotope of Pu Initially Present (Note That Pu-241 Data Includes Buildup of Am-241) 5-18

Figure 6-1. Detailed Model of a Single Package 6-5
Figure 6-2. Simplified Model of a Single Package 6-6
Figure 6-3. End-Impact Damaged Package Model 6-9
Figure 6-4. Side-Impact Damaged Package Model 6-10
Figure 6-5. HAC Single Package Model for 10 CFR 71.55(f) Analysis 6-11
Figure 6-6. Sensitivity of k_{eff} to Steel Density 6-15
Figure 6-7. Single Package Moderation Study 6-19
Figure 6-8. Normal Conditions of Transport – Square-Pitched Array 6-22
Figure 6-9. Normal Conditions of Transport – Square-Pitched Array Results 6-23
Figure 6-10. Normal Conditions of Transport – Hexagonal-Pitched Array 6-24
Figure 6-11. Normal Conditions of Transport – Hexagonal-Pitched Array Results 6-25

Figure 6-12. Damaged Packages – Side-Impact Hexagonal-Pitch Array, Top View 6-27
Figure 6-13. Damaged Packages – Side-Impact Square-Pitch Array, Top View 6-28
Figure 6-14. Damaged Packages – Side-Impact Nested Arrangement No. 1, Top View 6-29
Figure 6-15. Damaged Packages – Side-Impact Nested Arrangement No. 2, Top View 6-30
Figure 6-16. Damaged Packages – End-Impact Array, Repeated Layers, Side View 6-30
Figure 6-17. Damaged Packages – End-Impact Array, Alternating Layers, Side View 6-31
Figure 6-18. Damaged Packages – End-Impact Arrays, Repeated and Alternating Layers, Top View 6-31
Figure 6-19. Damaged Package Array Study 6-32
Figure 6-20. Damaged Package Array Internal (redwood zone) Moderation Study 6-33
Figure 6-21. Damaged Package TB-1 Location Study 6-34
Figure 6-22. Damaged Package External Moderation Study 6-35
Figure 6-23. Damaged Package External Moderation Study (Package Spacing Varied) 6-36
Figure 6-24. Single Package HAC for Air Transport 6-38
Figure 6-25. Pu Metal Sphere Critical Benchmark Histogram 6-52
Figure 6-26. Solution Lattice Critical Benchmark Histogram 6-54
Figure 6-27. Single Unit Solution Critical Benchmark Histogram 6-55
Figure 6-28. Dry Lattice Critical Benchmark Histogram 6-56
Figure 6-29. USLSTATS Plot for HEXSDRY Application of ck vs. k_{eff} 6-57
Figure 6-30. USLSTATS Plot for OCTSDRY Application of ck vs. k_{eff} 6-58
Figure 6-31. Spherical Segment Volume Calculations 6-62

Figure 7-1. Assembled PAT-1 Showing AQ-1, TB-1, and T-Ampoule 7-2

LIST OF TABLES

Table 1-1. Payload and Contents Configurations 1-13

Table 2-1. Weight of Plutonium Metal Contents and -Ampoule and Packing for Six Loading Configurations. 2-2
Table 2-2. Load Combinations for NCT and HAC 2-5
Table 2-3. Allowable Stresses for NCT and HAC Based on Regulatory Guide 7.6 (Room Temperature) 2-6
Table 2-4. Allowable Stresses for NCT and HAC Based on Regulatory Guide 7.6, (Elevated Temperatures) 2-7
Table 2-5. Approximate Weights of PAT-1 Package Components 2-9
Table 2-6. Listing of Material for Each Component in the Finite Element Models 2-11
Table 2-7. Normal Conditions of Transport (NCT) Impact Analyses (6), Components, and Orientations 2-26
Table 2-8. Hypothetical Accident Condition (HAC) Dynamic Crush Analyses (20), Components, and Orientations 2-26
Table 2-9. High Velocity (Aircraft) Impact Analyses (27), Components, and Orientations 2-27
Table 2-10. 30-ft Drop Impact Analyses (3), Components, and Orientations 2-28
Table 2-11. High Velocity (Aircraft) Impact Analyses Peak Tearing Parameter Values 2-30
Table 2-12. Redwood Orthotropic Crush Model Parameters 2-39

Table 2-13. Power-Law Hardening Constitutive Model Parameters 2-41
Table 2-14. Listing of Material for Each Components in the Finite Element Models..... 2-75
Table 2-15. Redwood Orthotropic Crush Model Parameters..... 2-76
Table 2-16. Maximum Strains in 4 ft End Drop Models 2-107
Table 2-17. Maximum Strains in 4 ft Side Drop Models..... 2-117
Table 2-18. Aircraft Accident Impact Analyses, Components, and Orientations..... 2-120
Table 2-19. High Velocity (Aircraft) Impact Analyses Peak Tearing Parameter Values 2-265
Table 2-20. Summary of Hypothetical Accident Condition (HAC) Dynamic Crush Analyses (20), Components, and Orientations 2-269
Table 2-21. 30-ft Drop Impact Analyses (3), Components, and Orientations 2-346

Table 3-1. Summary of Temperatures Under NCT and HAC 3-4
Table 3-2. Summary of Maximum Pressures inside the T-Ampoule for NCT and HAC..... 3-4
Table 3-3. Thermophysical Properties Used to Represent Redwood 3-5
Table 3-4. Thermophysical Properties of the Titanium Ampoule (Ti 6Al-4V)..... 3-6
Table 3-5. Service Temperatures of Packaging Components and Content Inside the TB-1 3-6
Table 3-6. Boundary Conditions Used for the "Heat" NCT Thermal Evaluation 3-9
Table 3-7. Comparison of Test and Analysis Temperatures – Low Temperature Test..... 3-11
Table 3-8. Boundary Conditions Used for the Transient Model Verification Exercise..... 3-16
Table 3-9. Grashof, Reynolds, Nusselt Numbers for Calm Wind, Open-Pool Fire Conditions..... 3-17
Table 3-10. Boundary Conditions Used for the HAC Thermal Evaluation..... 3-23
Table 3-11. Summary of Maximum Temperatures and Times for the HAC..... 3-27

Table 4-1. PAT-1 Package Post-Test Containment 4-3
Table 4-2. 831 g (1.83 lb): 3,000 A2 Quantity of ER Plutonium Metal Assuming No Pu-241 Decay..... 4-6
Table 4-3. 707 g (1.56 lb): 3,000 A2 Quantity of ER Plutonium Metal Assuming 100% Pu-241 Decay..... 4-6
Table 4-4. 676 g (1.49 lb): Alloyed Plutonium Metal Assuming 100% Pu-241 Decay 4-7
Table 4-5. 676 g (1.49 lb): Alloyed Plutonium Metal Assuming No Pu-241 Decay..... 4-7
Table 4-6. 60 g (0.13 lb): Bonded Pu/Be Metal Disk Assuming 100% Pu 241 Decay 4-8

Table 5-1. Summary Table of External Radiation Levels (Non-Exclusive Use)..... 5-2
Table 5-2. Plutonium Isotopics Used for Source Generation 5-3
Table 5-3. Gamma-Ray Source Used in the Shielding Analysis (2197 g Pu) 5-4
Table 5-4. Neutron Source Used in the Shielding Analysis (2197 g Pu)..... 5-5
Table 5-5. Dimensions of Materials Regions Used in Shielding Analyses 5-8
Table 5-6. Elemental Compositions Used in Shielding Analysis 5-9
Table 5-7. Neutron Flux-to-Dose Conversion Factors Used in Shielding Analysis..... 5-12
Table 5-8. Gamma Flux-to-Dose Conversion Factors Used in Shielding Analysis 5-13
Table 5-9. Source Geometry Optimization Dose Results (at PAT-1 Side Surface) 5-14
Table 5-10. Pu Isotope Wt % Under Various Depletion Scenarios 5-19
Table 5-11. Bounding Pu Isotope Mass Fraction Used in This Study..... 5-20

Table 5-12. Estimation of Degree of Overprediction in Bounding Pu Source Used in This Study 5-20
Table 5-13. Pu/Be Source Specification Used in This Study 5-21
Table 5-14. Neutron Source Spectrum Used in the Pu/Be Source Shielding Analysis 5-22

Table 6-1. Summary Table of Criticality Evaluation Results 6-2
Table 6-2. Material Specifications 6-11
Table 6-3. Stainless Steel PH 13-8 Mo Composition (wt %) 6-14
Table 6-4. Detailed Model, Plutonium Metal Sphere, Modeling Impact Study 6-20
Table 6-5. Detailed Model, Plutonium and Water Solution Cylinder, Modeling Impact Study 6-21
Table 6-6. Summary of Similarity Between Benchmark Configurations and Applications 6-46
Table 6-7. USL and Bias Data Summary 6-58
Table 6-8. List of Validation Critical Configurations 6-63
Table 6-9. Comparison of Tsunami Sensitivities and Direct Perturbation Sensitivities for a Representative Selection of Benchmark Critical Configurations 6-67
Table 6-10. Comparison of Direct Perturbation Sensitivities and Tsunami Sensitivities for the 11 Representative Applications 6-68
Table 6-11. Comparison of METAL SPHERE Applications to Critical Benchmarks 6-68
Table 6-12. Comparison of SOLUTION LATTICE Applications to Critical Benchmarks 6-69
Table 6-13. Comparison of SINGLE UNIT SOLUTION Applications to Critical Benchmarks 6-71
Table 6-14. Comparison of DRY LATTICE Applications to Critical Benchmarks 6-75
Table 6-15. Tabulation of Calculations Supporting the Standard Single Package Analysis for Normal Conditions of Transport and Hypothetical Accident Conditions 6-77
Table 6-16. Tabulation of Calculations Supporting the Analysis of Arrays of Undamaged Packages 6-87
Table 6-17. Tabulation of Calculations Supporting the Analysis of Arrays of Damaged Packages 6-102
Table 6-18. Tabulation of Calculations Supporting the Analysis of a Single Package of Fissile Material Intended for Air Transport 6-108
Table 6-19. Scoping Calculation Results for Single Packages 6-118
Table 6-20. Scoping Calculation Results for Normal Conditions of Transport Arrays 6-119
Table 6-21. Scoping Calculation Results for Hypothetical Accident Condition Arrays 6-120
Table 6-22. Scoping Calculation Results for Single Package, Air Transport Accident Provision 6-121
Table 6-23. Additional Scoping Calculation Results for Hypothetical Accident Condition Arrays 6-122

Table 7-1. Replacement Parts for the PAT-1 Packaging with *T-Ampoule Assembly* 7-6
Table 7-2. Parts List for T-Ampoule Loading 7-8
Table 7-3. Parts List for Loading the T-Ampoule into the TB-1 7-13

Table 7-4. Parts List for Loading the TB-1 Containment Vessel into the AQ-1 Overpack 7-16

Table 8-1. T-Ampoule Components 8-1
Table 8-2. Acceptance Tests for T-Ampoule Components 8-3

Table 9-1. Relationship between QA Implementing Documents and Elements of 10 CFR 71, Subpart H 9-4
Table 9-2. Project Tasks and Quality Categories for PAT-1 Addendum 9-8
Table 9-3. QA Categories for Design and Procurement of T-Ampoule Assembly and Inner Packing 9-8
Table 9-4. Level of QA Control Per QA Element 9-9

This page intentionally left blank

1. GENERAL INFORMATION

1.1 Introduction

The Plutonium Air Transportable Package, Model PAT-1, is certified under Title 10, Code of Federal Regulations Part 71[1] by the U.S. Nuclear Regulatory Commission (NRC) per Certificate of Compliance (CoC) USA/0361B(U)F-96, (currently Revision 9).[2]

The primary components of the currently certified PAT-1 configuration include the PC-1 stainless steel inner container, the TB-1 stainless steel containment vessel (*Containment Vessel*[A] Drawing 1017, designated TB-1), and the AQ-1 protective overpack assembly (*Overpack, AQ*, Drawing 1002, designated AQ-1). The *Safety Analysis Report for the Plutonium Air Transportable Package, Model PAT-1*, NUREG-0361,[2,3] as supplemented by Issue B of Drawings 1004, 1009, 1013, 1016, 1017, 1018, 1019, 1020 and 1022, provides detailed material specifications and drawings of the current PAT-1 packaging components, and demonstrates compliance with 10 CFR 71.[1] Issue B versions of Drawings 1004, 1009, 1013, 1016, 1017, 1018, 1019, 1020 and 1022 are listed and provided in Section 1.3.2 of this Safety Analysis Report (SAR) Addendum. The current authorized contents are plutonium oxide (PuO_2) and its daughter products, or a mixture of PuO_2 and uranium oxide (UO_2) and its daughter products, as further described in CoC USA/0361/B(U)F-96 Revision 9, Section 5.[2]

The purpose of this SAR Addendum is to incorporate plutonium (Pu) metal as a new payload for the PAT-1 package. The Pu metal is packed in an inner container (*T-Ampoule Assembly*, Drawing 2A0261, designated the T-Ampoule) that replaces the PC-1 inner container. The T-Ampoule and associated Pu metal contents packing configurations are further described in Section 1.2.1 and Section 1.2.2 of this addendum, respectively.

Based on the proposed maximum content of 831 g (1.83 lb) of plutonium metal, the PAT-1 with T-Ampoule is designated a Category I, Type B fissile material package, and the Criticality Safety Index (CSI) is 0.1. The Transportation Index (TI) is based on the maximum radiation level at a distance of 1 m (39.4 in.) from the external surface of the package and will be established each time a PAT-1 package is loaded with approved content. The actual TI measured at the time of shipment can be no greater than the calculated value of 2.5 (see Table 5-1). All other PAT-1 packaging component designs, currently authorized content mass and form, and 25 watt (85.3 Btu/hr) maximum decay heat remain unchanged from that documented in NUREG-0361.[3]

The documentation and results from analysis contained in this addendum demonstrate that the replacement of the PC-1 and associated packaging material with the T-Ampoule and associated packaging, and the addition of the plutonium metal content, are not significant with respect to the design, operating characteristics, or safe performance of the containment system and prevention of criticality when the package is subjected to the tests specified in 10 CFR 71.71, 71.73 and 71.74.

The Quality Assurance Program requirements for the PAT-1 package and the T-Ampoule are discussed in Section 9 of this addendum.

[A] The drawing titles are in italics and are used interchangeably with the designated names in this addendum. See Section 1.3.2 in this addendum and Chapter 9 in the SAR[3] for drawing number, title, and revision.

1.2 Package Description

1.2.1 Packaging

Details for the PAT-1 packaging components: AQ-1 overpack, TB-1 containment vessel, PC-1 inner container, and associated packing materials (which are unaffected by the packaging component design and content modifications addressed in this addendum), are contained in NUREG-0361 as supplemented by Issue B of Drawings 1004, 1009, 1013, 1016, 1017, 1018, 1019, 1020 and 1022.

The difference between the PAT-1 with T-Ampoule configuration (see Figure 1-1) and the currently certified PAT-1 with PC-1 configuration is the PAT-1 with T-Ampoule configuration (see *PAT-1/TB-1/T-Ampoule Assembly* [Drawing R99794 in this addendum] and *TB-1/ T-Ampoule Shipping Vessel Assembly* [Drawing 2A0263 in this addendum]) consists of (1) a *T-Ampoule* (see Figure 1-2 and Drawing 2A0261 listed in Section 1.3.2) containing plutonium metals in the configurations illustrated in Figures 1-3 through 1-5, and (2) the *Ring, Filler* (Drawing 2A0262, designated Ring Filler). The PAT-1 with PC-1 configuration consists of the PC-1, aluminum honeycomb spacer, 2000 g (4.41 lb) authorized content, and associated packing material. The weight of the PAT-1 packaging for plutonium oxide is presented in Section 1.2.1 and Section 2.2 of the SAR. The approximate weights from the SAR for the AQ-1 overpack, TB-1 containment vessel, PC-1 Product Can (including aluminum spacer), and contents is 225 kg (496 lb). The PAT-1 with T-Ampoule configuration is limited to the current certified TB-1 gross payload weight of 2100 g (4.7 lbs).

1.2.1.1 Ring Filler

The Ring Filler is used to fill the void space between the top of the T-Ampoule and the TB-1 closure lid. The Ring Filler is 10.72 cm (4.22 in.) in diameter, 1.27 cm (0.5 in.) thick, and is manufactured of titanium (Ti) alloy 6A1-4V (hereafter referred to as Ti-6A1-4V, Grade 5).

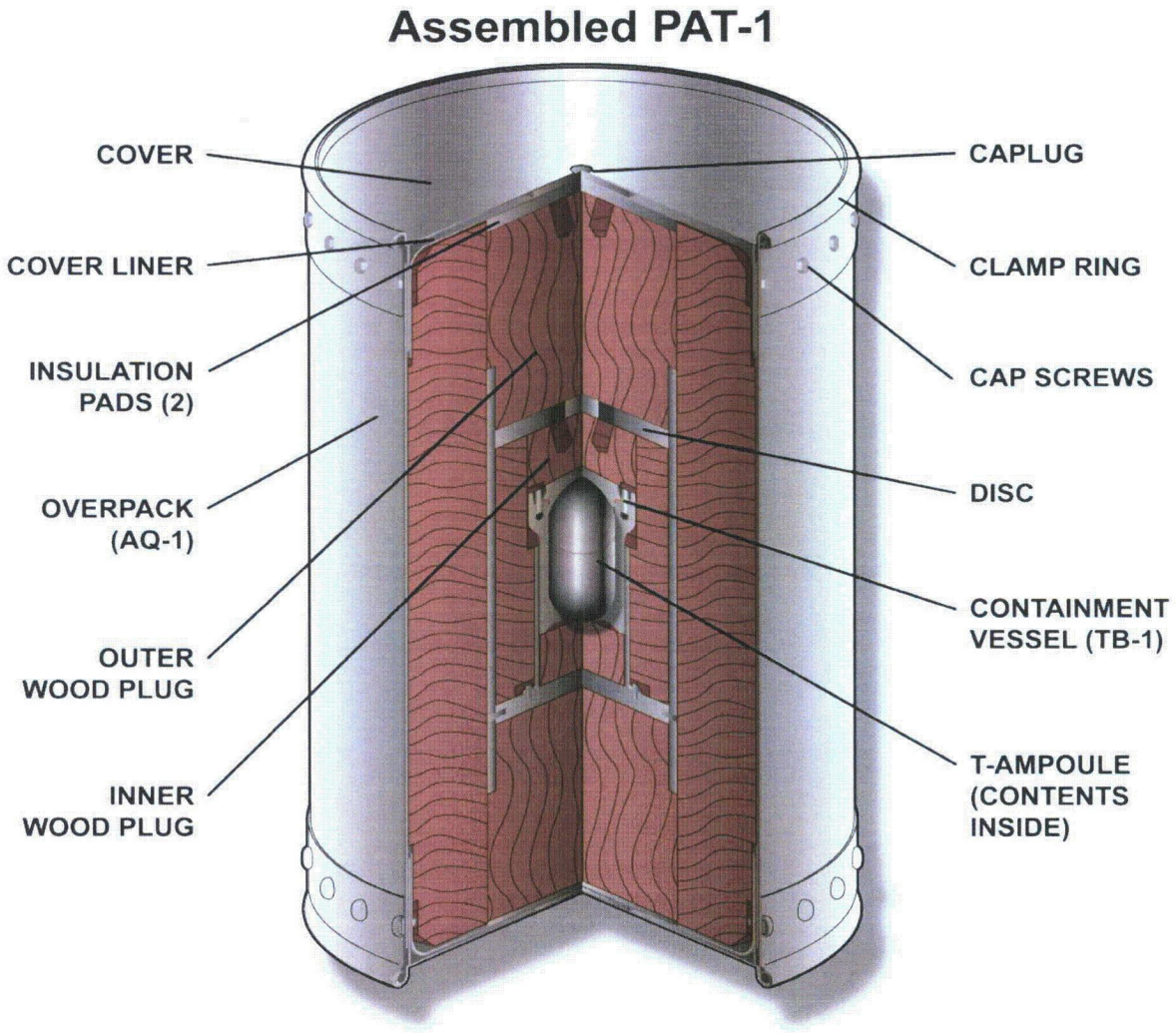

Figure 1-1. Assembled PAT-1 Showing AQ-1, TB-1, and T-Ampoule

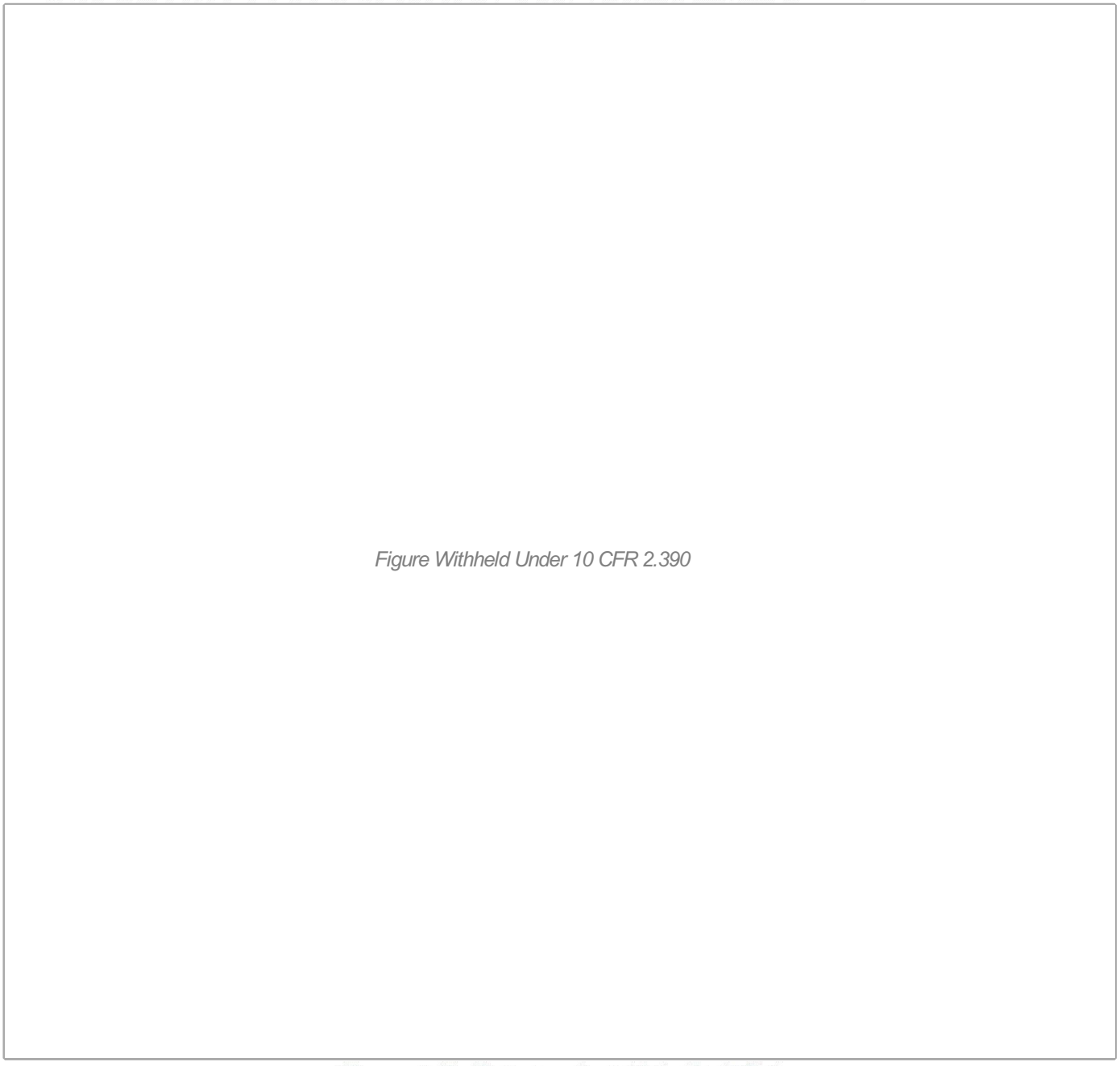

Figure 1-2. T-Ampoule within the TB-1

1.2.1.2 T-Ampoule and Internal Packing

The T-Ampoule's primary components consist of a body (bottom), lid (top), and elastomeric Viton® O-ring. The *Body, T-Ampoule* (Drawing 2A0259, designated T-Ampoule Body), and *Lid, T-Ampoule* (Drawing 2A0260, designated T-Ampoule Lid) are fabricated to a nominal wall thickness of 1.5875±0.0635 mm (0. 0625±0.0025 in.) from solid billets of Ti-6A1-4V, Grade 5. The PAT-1040 *Titanium and O-Ring and Component Fabrication Specification* in Section 1.3.3.1 provides the manufacturing and quality assurance specification for the T-Ampoule, Filler Ring, *Inner Cradle* (Drawing 2A0385, designated Inner Cradle), *Sample Container-1 (SC-1) Assembly* (Drawing 2A0268, designated SC-1), *Sample Container-2 (SC-2) Assembly* (Drawing 2A0265 designated SC-2), and O-rings for the T-Ampoule, SC-1 and SC-2. Ti-6A1-4V, Grade 5 was selected for its high strength, light weight, and high resistance to eutectic reaction with plutonium metal. The T-Ampoule has a smooth finish on the interior and exterior surfaces to facilitate decontamination, and its body and lid sections are joined together and sealed using a screw-thread joint with an elastomeric Viton® O-ring bore seal to maintain content quality.

The T-Ampoule's internal packing consists of:

1. A nested two-sample-container configuration (see Figure 1-3) SC-2, including one spacer) packed and supported by a titanium Inner Cradle, or
2. A nested three-sample-container configuration (see Figure 1-4) SC-1, including two spacers) packed and supported by a titanium Inner Cradle, or
3. A Pu hollow cylinder (Figure 1-5, also designated plutonium metal hollow cylinder) with or without tantalum foil wrapped around the outside of the cylinder (and having the free ends of the foils tucked into the cylinder). The Pu hollow cylinder may or may not be surrounded by crushed/crumpled foil and/or copper foam depending on the operational needs.

The plutonium metal contents may be wrapped with tantalum foil or not wrapped based on operational need and/or packed with copper (Cu) foam before they are loaded in SC-1 or SC-2 sample containers. The tantalum foil ranges in thickness from 0.00254 cm (0.001 in.) to 0.0229 cm (0.009 in.), and the minimum purity ranges from 99.75% (3N5), to 99.98% (3N8), or to 99.99% (4N). As a packing option, the bare or tantalum-foil-wrapped plutonium metal contents may be packed in the sample containers using Cu foam pieces. The Cu foam material is high-purity Cu foam shapes with a minimum of 1.24 MPa (180 psi) compressive strength and nominal 9.5 percent relative density.

For packing the Pu hollow cylinder content, tantalum foil may be used, but is not required. The plutonium metal contents contained in the T-Ampoule and its packing is described in the following section.

1.2.2 Contents

The plutonium metal contents contained within the T-Ampoule in the TB-1 containment vessel of the PAT-1 package are limited by the following requirements:

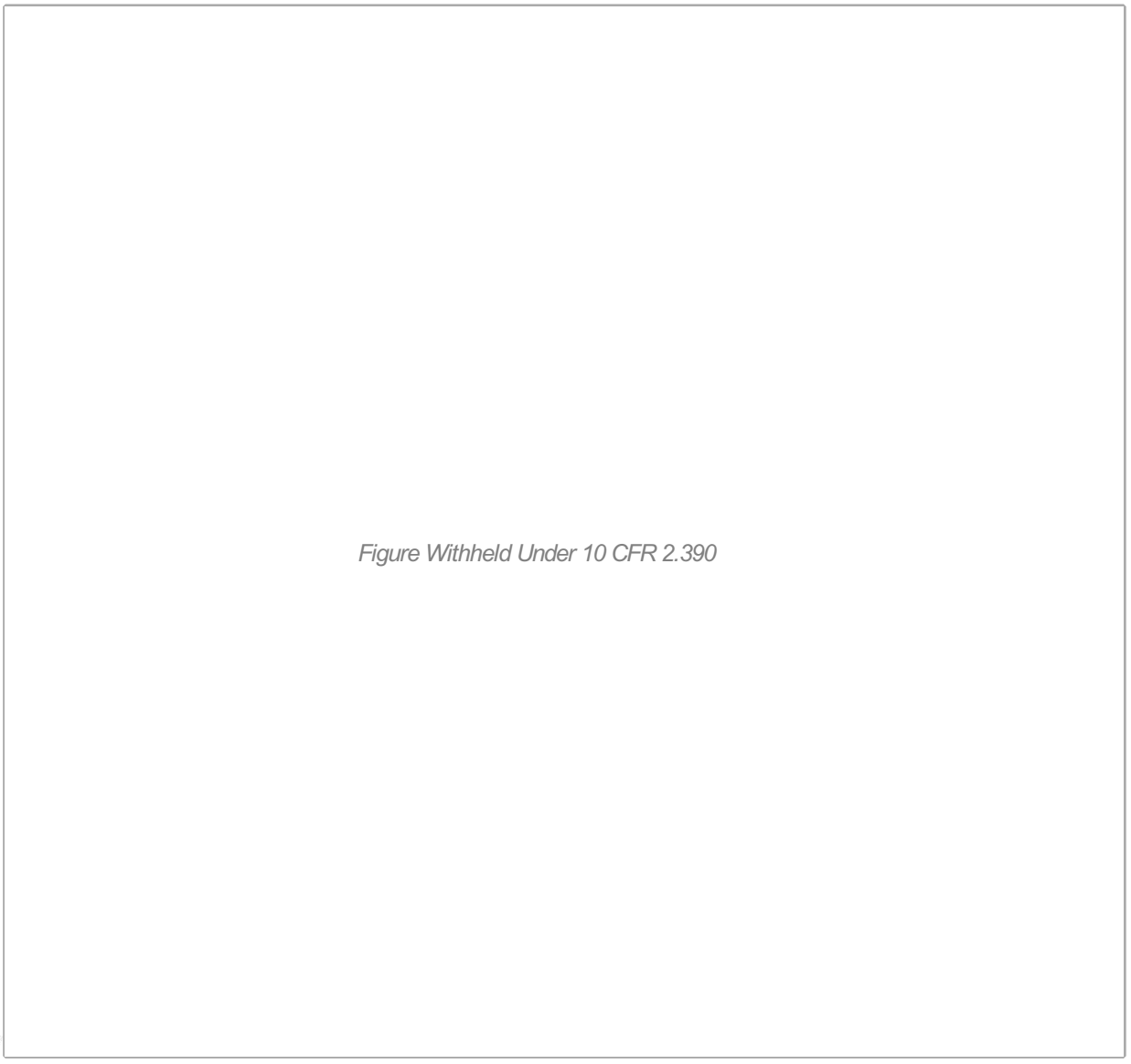

Figure 1-3. Two Sample Containers (SC-2) Nested within T-Ampoule and TB-1

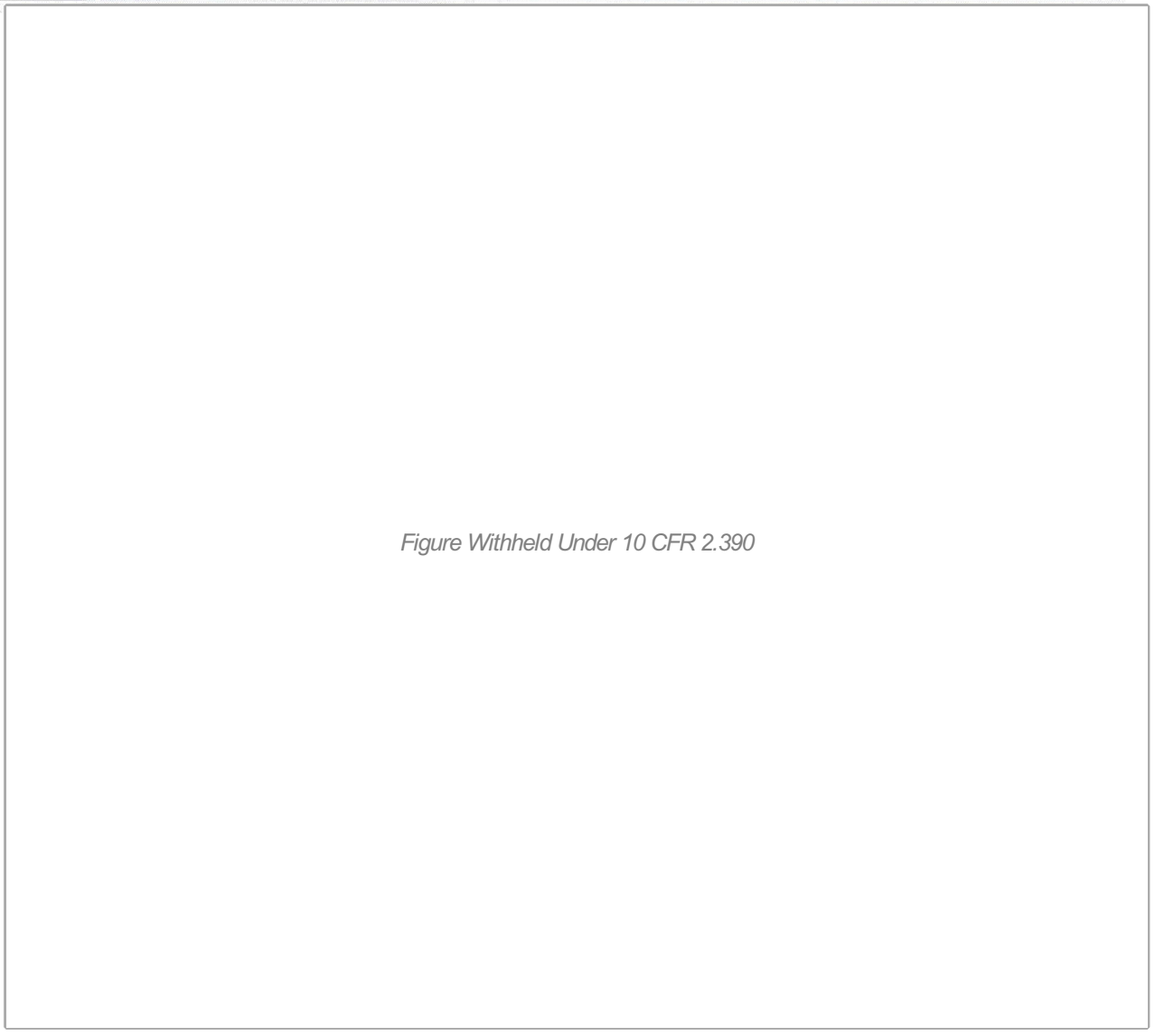

Figure 1-4. Three Sample Containers (SC-1) Nested within T-Ampoule and TB-1

Figure 1-5. 831 gram (1.83 lb) Pu Hollow Cylinder within T-Ampoule and TB-1

a. Material Description

- Material type: The T-Ampoule and its packing will hold plutonium metal in various isotopic compositions and composite (Pu and beryllium [Be] separated by a titanium layer) material.[4] The plutonium metal compositions, decay heat, activity and A_2 are listed below for the largest content of the Pu hollow cylinder, alloyed samples and composite materials:
  - 831 g (1.83 lb) Pu Hollow Cylinder – alpha or delta phase, information for 3000 A_2 quantity of Electro-refined (ER) plutonium metal assuming no Pu-241 decay, 829.67 g (1.83 lb) Pu is shown below. The minimum weight of the Pu hollow cylinder is 731 g (1.61 lb) Pu.

831 grams: **3,000 A_2** quantity of ER Pu metal assuming no Pu241 decay									
Metal Mass (g) (max)	Mass % (max)	Grams (max)	LANL Specification 55Y-638728	Isotope	Pu Isotopic % (max)	Pu Isotopic mass (g)	Decay Heat (W)	Activity (Ci)	A^2
831.00	Plutonium 99.84%	Plutonium 829.67		Pu238	0.05%	0.41	2.35E-01	7.05E+00	2.61E+02
				Pu239*	92.35%	766.20	1.46E+00	4.75E+01	1.76E+03
				Pu240	6.50%	53.93	3.83E-01	1.24E+01	4.59E+02
				Pu241	1.00%	8.30	1.04E-01	8.30E+02	5.19E+02
				Pu242	0.10%	0.83	8.30E-05	3.24E-03	1.20E-01
				Am241	0.00%	0.00	0.00E+00	0.00E+00	0.00E+00
	Impurities 0.16%	Impurities 1.33		Impurities: N/A					
* stated as % balance						Total:	2.18E+00	8.97E+02	3.00E+03

- 676 g (1.49 lb) Maximum Content in SC-2 Sample Container – Alloyed plutonium metal assuming no Pu-241 decay and 100% Pu-241 decay, 668.16 g (1.47 lb) Pu. Note: the SC-2 sample container configuration has the highest plutonium content within the TB-1 for the sample containers.

676 grams: Alloyed Pu metal assuming no Pu241 decay									
Metal Mass (g) (max)	Mass % (max)	Grams (max)	LANL Specification 55Y-638728	Isotope	Pu Isotopic % (max)	Pu Isotopic mass (g)	Decay Heat (W)	Activity (Ci)	A^2
676.00	Plutonium 98.84%	Plutonium 668.16		Pu238	0.05%	0.33	1.89E-01	5.68E+00	2.10E+02
				Pu239*	92.35%	617.04	1.17E+00	3.83E+01	1.42E+03
				Pu240	6.50%	43.43	3.08E-01	9.99E+00	3.70E+02
				Pu241	1.00%	6.68	8.35E-02	6.68E+02	4.18E+02
				Pu242	0.10%	0.67	6.68E-05	2.61E-03	9.65E-02
				Am241	0.00%	0.00	0.00E+00	0.00E+00	0.00E+00
	Impurities 0.16%	Impurities 1.08		Impurities: N/A					
	Gallium 1.00%	Gallium 6.76		Gallium: N/A					
* stated as % balance						Total:	1.75E+00	7.22E+02	2.41E+03

676 grams: Alloyed Pu metal assuming 100% Pu241 decay									
Metal Mass (g) (max)	Mass % (max)	Grams (max)	LANL Specification 55Y-638728	Isotope	Pu Isotopic % (max)	Pu Isotopic mass (g)	Decay Heat (W)	Activity (Ci)	A^2
676.00	Plutonium 98.84%	Plutonium 668.16		Pu238	0.05%	0.33	1.89E-01	5.68E+00	2.10E+02
				Pu239*	92.35%	617.04	1.17E+00	3.83E+01	1.42E+03
				Pu240	6.50%	43.43	3.08E-01	9.99E+00	3.70E+02
				Pu241	0.00%	0.00	0.00E+00	0.00E+00	0.00E+00
				Pu242	0.10%	0.67	6.68E-05	2.61E-03	9.65E-02
				Am241	1.00%	6.68	7.67E-01	2.27E+01	8.41E+02
	Impurities 0.16%	Impurities 1.08		Impurities: N/A					
	Gallium 1.00%	Gallium 6.76		Gallium: N/A					
* stated as % balance						Total:	2.44E+00	7.66E+01	2.84E+03

- 60 g (0.13 lb) per disk – Bonded Pu/Be metal disc assuming 100% Pu-241 decay, 52.2 g (0.115 lb) Pu, 7.80 g (0.172 lb) Be (includes alpha barrier between Pu and Be). Composition, decay heat, activity, and A_2 for other shapes would be similar.

60 grams: Bonded Pu/Be metal disc assuming 100% Pu241 decay

Composite %	Metal Mass (g) (max)	Mass % (max)	Grams (max)		Isotope	Pu Isotopic % (max)	Pu Isotopic mass (g)	Decay Heat (W)	Activity (Ci)	A^2
Pu metal 87.00%	52.20	MT52 Plutonium 98.84%	MT52 Plutonium 51.59	LANL Specification 51Y-638728	Pu238	0.05%	0.03	1.46E-02	4.39E-01	1.62E+01
					Pu239*	92.35%	47.65	9.05E-02	2.95E+00	1.09E+02
					Pu240	6.50%	3.35	2.38E-02	7.71E-01	2.86E+01
					Pu241	0.00%	0.00	0.00E+00	0.00E+00	0.00E+00
					Pu242	0.10%	0.05	5.16E-06	2.01E-04	7.45E-03
					Am241	1.00%	0.52	5.92E-02	1.75E+00	6.50E+01
		Impurities 0.16%	Impurities 0.08		Impurities: N/A					
		Gallium 1.00%	Gallium 0.52		Gallium: N/A					
Beryllium 13.00%	7.80	Beryllium 13.00%	Beryllium 7.80		Beryllium: N/A					
Alpha Barrier 0.00%	0.00	Alpha Barrier 0.00%	Alpha Barrier 0.00		Assumes no alpha barrier to yield maximum dose					
100.00%	60.00	◄◄◄ Totals ►►►						1.88E-01	5.92E+00	2.19E+02
*stated as % balance										

Dose rate calculations:

- Material form: The plutonium metal must be in solid form (may be pure, alloyed or composite)[5] with a small amount of surface oxides. Material shapes are provided below:
  - Hollow right-circular cylinders of Pu metal as specified in Table 1-1,
  - Various geometric shapes of alloyed Pu metal, including (1) circular discs of varying diameters and thicknesses, (2) rectangular strips of varying lengths, widths, and thicknesses, (3) cylinders in sizes and masses up to those used in the structural analysis, (4) random shapes used for chemistry analysis, and (5) composites as specified in Table 1-1.

- Material quantity: The maximum mass of the plutonium metal (fissile material) contained in the T-Ampoule is 831 g (1.83 lb). The maximum quantity and range for each content and packing configuration is shown in Table 1-1:
  - There are two configurations of Pu hollow cylinders. The maximum cylinder weight has a metal mass of 831 g (1.83 lb) (see Figure 1-5). The minimum hollow cylinder weight has a metal mass of 731 g (1.61 lb). The Pu hollow cylinders may be positioned anywhere within the T-Ampoule.
  - Each SC-2 sample container can carry up to 338 g (0.75 lb) of plutonium metal, and each SC-1 sample container can carry up to 174 g (0.38 lb) of plutonium metal. The sample containers are supported within the T-Ampoule by the Inner Cradle as shown in Figures 1-3 and 1-4. The T-Ampoule with its packing and contents is limited to the current certified TB-1 gross payload weight of 2100 g (4.7 lb). The plutonium metal contents may be positioned anywhere in the sample container (SC-1 or SC-2), as applicable.

For the composite Pu/Be samples, each sample container (SC-1 or SC-2) may contain up to 60 g (0.132 lb) each. The total composite mass is 120 grams (0.264 lb) for the two SC-2 configuration and 180 g (0.397 lb) for the three SC-1 configuration.

- Density of Plutonium: Both alpha and delta density plutonium and composite Pu/Be material may be shipped. The densities used for the structural analysis are presented below:
  - Alpha and delta phase: 19.8 g/cc (0.716 lb/in^3)
  - Composite Pu/Be: 15.9 g/cc (0.5745 lb/in^3)

  Page 103 of the Plutonium Handbook[6] published by the American Nuclear Society lists various densities for the different phases of plutonium (see Table 5.1 in the Handbook). These are calculated densities from x-ray diffraction measurements of lattice spacings and represent "theoretical" values for unalloyed plutonium (at temperatures where they are in equilibrium). Several caveats affect the density of "real" Pu. For delta phase at ambient temperature, some alloying elements must be added to stabilize this phase and thus, lowers the theoretical density to below 15.92 g/cc (this value is at a nominal temperature of 320°C). For alpha phase (unalloyed) at ambient temperature, typical as-cast densities of high-quality temperature phases range from 19.4 to 19.7 g/cc due to three factors: typical impurities, retained higher temperature phases with lower density, and microcracking due to residual stresses. For the structural analysis in Section 2 of this addendum, a value of 19.8 g/cc (0.716 lb/in^3) is used for both the alpha and delta phase plutonium. For the composite Pu/Be material, the density of the delta phase plutonium 15.9 g/cc (0.5745 lb/in^3) is conservatively used in the structural analysis presented in Section 2 of this addendum.
- Chemical form: The chemical form of the plutonium is metal, with possible surface oxides, PuO_2. The metal may be alloyed with gallium.
- Nonfissile materials used as neutron absorbers or moderators: There are no nonfissile materials used as neutron absorbers or moderators.
- Materials subject to chemical, galvanic, or other reactions, including generation of gases: The plutonium metal contents may be subject to oxidation in air (see Section 4.5.2 in this addendum for estimate of oxidation). Eutectic formation between the plutonium metal contents and the iron in the TB-1 is prevented by a eutectic barrier made of titanium. See Section 3.5.2 in this addendum for discussion of eutectics. The O-rings in the TB-1, T-Ampoule, and SC-1 or SC-2 sample containers are subject to volatilization in a plutonium air transport accident fire, and the pressure generation discussed in Section 4.5.4 of this addendum. The plutonium will decay, forming helium gas. The gas generation is discussed in Section 4.5.3.
- Moisture content: The T-Ampoule, SC-1 or SC-2 sample containers, and radioactive materials will be assembled in a typical glove box and/or laboratory with a standard line atmosphere consisting of nitrogen (N), argon (Ar), or helium (He) inert gas, with an oxygen content not exceeding 0.5% and water content not exceeding 20 ppm.
- Internal decay heat: The isotopic composition of all contents must be such that a thermal activity of 25 watts (85.3 Btu/hr) is not exceeded while the contents are in the PAT-1 package.

b. Additional Requirements

- The T-Ampoule must be used for Pu metal shipments.
- Sample containers (SC-1 of SC-2) may be used within the T-Ampoule only if supported by the Inner Cradle as shown in Figures 1-3 and 1-4.
- Sample containers may include copper foam or tantalum foil as packing materials for Pu.
- The Pu hollow cylinder may be wrapped with tantalum foil or not wrapped based on operational need and packed with copper foam.
- The ER hollow cylinder may be wrapped with tantalum foil or not wrapped based on operational need and packed with copper foam.
- The total weight of the Ring,Filler, T-Ampoule, packing materials (Cu foam, tantalum foil), elastomeric O-rings, SC-1 or SC-2 sample containers and Inner Cradle (if used), and Pu metal shall not exceed 2100 g (4.7 lb).
- The Ring Filler must be used with the T-Ampoule.

1.2.2.1 Plutonium Contents and Packing

Plutonium metal contents carried within the T-Ampoule and sample containers include the following configurations:

- Various geometric shapes of alloyed Pu metal, including (1) circular discs of varying diameters and thicknesses, (2) rectangular strips of varying lengths, widths, and thicknesses, (3) cylinders in sizes and masses up to those used in the structural analysis, (4) random shapes used for chemistry analysis, and (5) composites as specified in Table 1-1.
- Hollow right-circular cylinders of alloyed plutonium metal specified in Table 1-1.
- Composite Pu/Be materials of different geometries.

The packing requirements are:

- The Inner Cradle must be used to position the SC-1 or SC-2 sample containers within the T-Ampoule.
- The hollow cylinders may be wrapped with tantalum foil for contamination control or not wrapped based on operational need and packed with crushed tantalum foil.
- Plutonium metal contents may be wrapped with tantalum foil for contamination control or not wrapped based on operational need and packed in the sample containers (SC-1 or SC-2).
- Plutonium metal contents may be packed with Cu foam (as required) within the sample containers (SC-1 or SC-2).

The payload and contents configurations are presented in Table 1-1.

Table 1-1. Payload and Contents Configurations

Payload Configuration	Total Plutonium Content Weight in T-Ampoule (g)	Dimensions of Plutonium Contents
Pu hollow cylinder[a] (Electro-Refined or alloyed) in *T-Ampoule Assembly*	731 to 831	6.350 cm (2.500 in.) OD, 5.801 cm (2.284 in.) ID x 7.087 cm (2.790 in.) length for 731 g payload to 6.350 cm (2.500 in.) OD, 5.801 cm (2.284 in.) ID x 8.054 cm (3.171 in.) length for 831 g payload Unilateral tolerances for the cylinder: -0.000 in./+0.010 in. applied to the outside diameter -0.010 in./+0.000 in. applied to the inside diameter
Sample Container-1 (SC-1) Assembly; up to 174 g alloyed delta phase Pu metal[b] in each container in *T-Ampoule Assembly*	0 to 523	Any configuration of plutonium metal, not to exceed maximum gross Pu weight specified per sample container. (Bounding analysis performed with a 2.23 cm (0.88 in.) OD x 2.23 cm (0.88 in.) long solid cylinder[b]).
Sample Container-2 (SC-2) Assembly up to 338 g alloyed delta phase Pu metal[b] in each container in *T-Ampoule Assembly*	0 to 676	Any configuration of plutonium metal, not to exceed maximum gross Pu weight specified per sample container. (Bounding analysis performed with a 2.79 cm (1.10 in.) OD x 2.79 cm (1.10 in.) long solid cylinder[b]).
Sample Container-1 (SC-1) Assembly, up to 60 g bonded Pu/Be metal content with alpha barrier[4] in each container in *T-Ampoule Assembly*	0 to 180	Composite content not to exceed 60 g[c] per sample container *SC-1*
Sample Container-2 (SC-2) Assembly, up to 60 g bonded Pu/Be metal content with alpha barrier[4] in each container in *T-Ampoule Assembly*	0 to 120	Composite content not to exceed 60 g[c] per sample container *SC-2*

[a] The Pu hollow cylinder may be wrapped in tantalum foil and placed in the T-Ampoule. Additional crushed tantalum foil may be used to pack around the hollow cylinder. Use of 10% relative density pure Cu foam to support the Pu hollow cylinder is optional. For the structural analysis in Section 2, the following bounding conditions are used:

1. For the 731 g cylinder, 6.375 cm (2.510 in.) OD, 5.776 cm (2.274 in.) ID x 6.490 cm (2.555 in.) length.
2. For the 831 g cylinder, 6.375 cm (2.510 in.) OD, 5.776 cm (2.274 in.) ID x 7.374 cm (2.903 in.) length.

[b] A solid cylinder shape in the analysis is assumed for the alloyed delta phase Pu content. The actual shape and number of pieces within the sample convenience container may vary, but cannot exceed the weight limit specified for each container. Tantalum foil may be used to wrap the samples as well as to provide additional packing. Use of 10% relative density pure Cu foam to support the samples is optional.

[c] The composite disc may be wrapped in tantalum foil with crushed tantalum foil as packing. Use of 10% relative density pure Cu foam to support the composite material is optional. The alternate configurations for the 60 gram content in an individual sample container include:

1. Multiple small cylinders approximately 5.1 mm (0.2") diameter x 5.1 mm (0.2") height at an individual mass of 1.7 grams and optionally clustered (35 each) for a total of 60 grams per sample container.
2. Multiple disks with varying diameters - (12 mm to 45 mm) and thickness (2.37 to 6 mm) with an individual mass range (10.8 to 59.9 grams) for a total of 60 grams per sample container.
3. A flat plate with varying thickness (up to 6 mm), fixed width (12.5 mm (0.49"), and variable length (30 mm to 50 mm) with an individual mass range (35.8 to 59.6 grams) individually loaded in a sample container.
4. Multiple "long" cylindrical specimens with a diameter range of 7.62 to 8.9 mm (0.3" to 0.35") with varying length (26 mm (1.02") to 60 mm (2.36") with an individual mass range of (18.9 to 59.3 grams) for a total of 60 grams per sample container.

1.2.3 Special Requirements for Pu

The Pu contents of the PAT-1 package specified in this addendum are of a solid metallic form and will remain in solid form following the testing specified in 10 CFR 71.73.

1.2.4 Operational Features

The operational features of the PAT-1 package (the AQ-1 overpack and the TB-1 containment vessel) require minimal instruction for assembly, disassembly, handling, and transport. The PAT-1 package is transported on its shipping skid and is loaded or unloaded by means of a sling and hoist or forklift with barrel clamp adapter as described in Section 7 of this addendum. Ordinary socket wrenches (3/8 and 5/8 inch) and open-ended adjustable wrenches are used to attach or remove the AQ-1 *Ring, Clamp Modified* (Drawing 1006, designated Clamp Ring). A soft-faced mallet may be used to loosen or install the removable covers if the assembly is tight. No tools are necessary, after this operation, to assemble or disassemble the other AQ-1 removable covers, plugs, load spreaders, and insulation pad, or to insert or remove the TB-1 containment vessel as described in Chapter 7 of the SAR. Only hand tools will be used to assemble or disassemble the TB-1. No use of power or pneumatic tools is authorized.

The physical operating features which assure TB-1 integrity following the 10 CFR 71 NCT, HAC, and accident conditions for air transport of plutonium are the TB-1 *Gasket Copper* (Drawing 1019, designated Copper Gasket), a fluorocarbon O-ring, and the TB-1 containment vessel. These features of the TB-1, when assembled to procedures described in Chapter 7 of the SAR and acceptance tested and maintained as described in Chapter 8 of the SAR, assure that the TB-1 will meet the containment acceptance criteria for test requirements in 10 CFR 71.71, 71.73, and 71.74.

The T-Ampoule is sealed with an elastomeric O-ring in a bore seal to maintain content quality. The container is designed to be tightened or loosened by hand or with aids such as strap wrenches, clamp fixtures, etc.

1.3 Appendix

1.3.1 References

1. United States. Nuclear Regulatory Commission. Code of Federal Regulations, 10 CFR 71, "Packaging and Transportation of Radioactive Material." January 1, 2009.

2. United States. Nuclear Regulatory Commission. "Certificate of Compliance for Radioactive Material Packages," Certificate Number 0361, Revision Number 9, Docket Number 71-0361, Package Identification Number USA/0361/B(U)F-96. March 4, 2009.

3. United States. Nuclear Regulatory Commission. NUREG-0361, "Safety Analysis Report for the Plutonium Air Transportable Package, Model PAT-1." Washington, D.C. 1978.

4. United States. Nuclear Regulatory Commission. NUREG-0360, "Qualification Criteria To Certify A Package For Air Transport Of Plutonium." Washington, D.C. 1978.

5. Caviness, M. L., and Rubin, J.B. "Authorized Contents Proposed for the Plutonium Air Transporter (PAT-1) Packaging (U)," LA-UR-08-05154. Los Alamos National Laboratory. Los Alamos, NM: August 7, 2008.

6. Wick, O. J., *Plutonium Handbook, A Guide to the Technology, Volume I*, Pacific Northwest Laboratories, Battelle Memorial Institute, The American Nuclear Society, La Grange Park, Illinois: 1980.

1.3.2 Drawings

Drawing Number	Title	Revision
1004	DRUM	B
1009	CYLINDER, WOOD	B
1013	PLUG, WOOD, REMOVABLE	B
1016	LOAD SPREADER ASSEMBLY	B
1017	CONTAINMENT VESSEL	B
1018	BOLT, SOCKET, HEAD SPECIAL .500-20	B
1019	GASKET COPPER	B
1020	LID, TB	B
1022	BODY, TB	B
R99794	PAT-1/TB-1/T-AMPOULE ASSEMBLY (U)	A
2A0263	TB-1/T-AMPOULE SHIPPING VESSEL ASSEMBLY (U)	A
2A0259	BODY T-AMPOULE (U)	A
2A0260	LID T-AMPOULE (U)	A
2A0261	T-AMPOULE ASSEMBLY (U)	A
2A0262	RING, FILLER (U)	A
2A0264	BODY SAMPLE CONTAINER-1 (SC-1) (U)	A
2A0265	SAMPLE CONTAINER-2 (SC-2) ASSEMBLY (U)	A
2A0266	BODY SAMPLE CONTAINER-2 (SC-2) (U)	A
2A0267	LID SAMPLE CONTAINER-1 (SC-1) (U)	A
2A0268	SAMPLE CONTAINER-1 (SC-1) ASSEMBLY (U)	A
2A0269	LID SAMPLE CONTAINER-2 (SC-2) (U)	A
2A0385	INNER CRADLE (U)	A

Figure Withheld Under 10 CFR 2.390

Figure Withheld Under 10 CFR 2.390

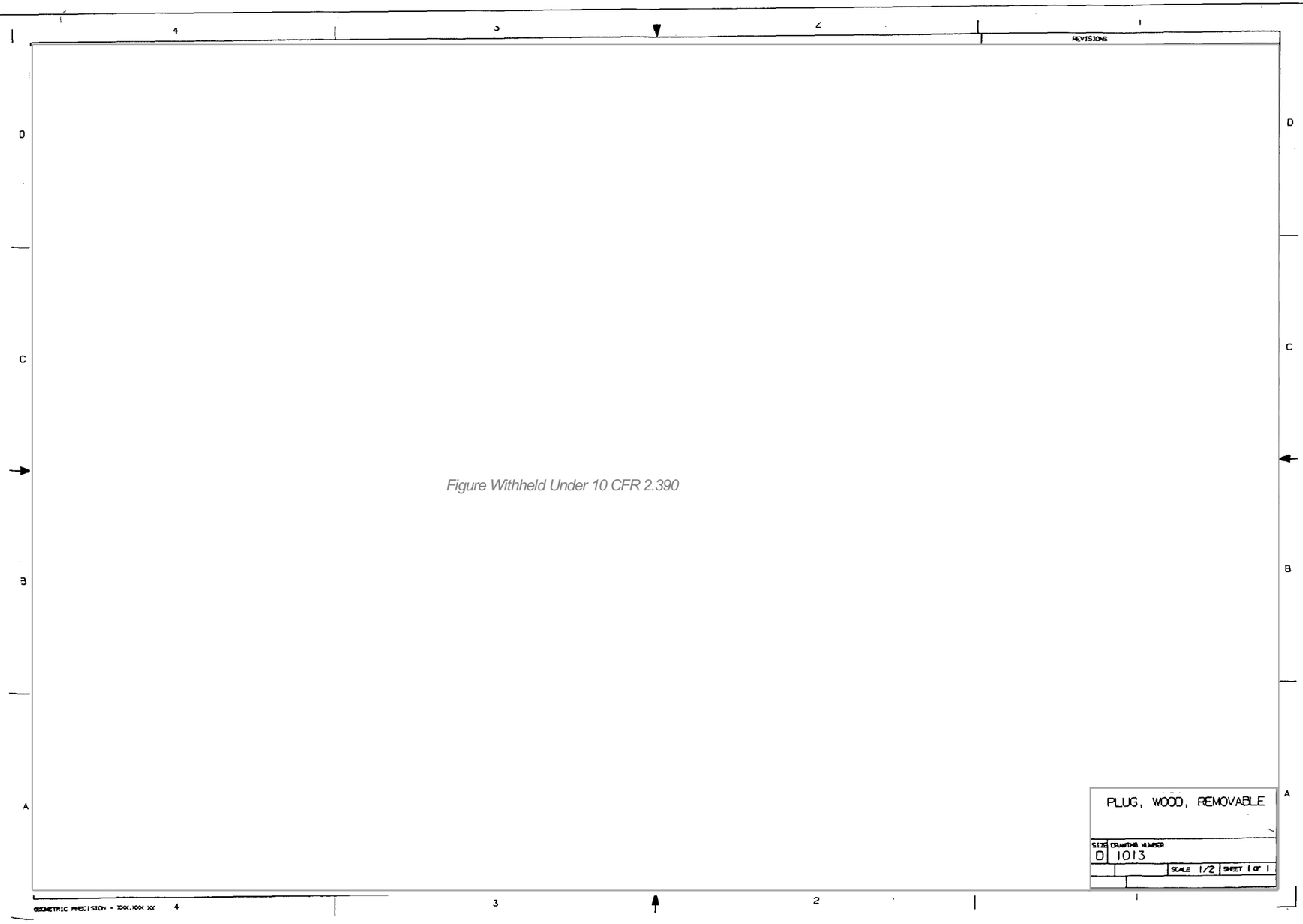
REVISIONS
Figure Withheld Under 10 CFR 2.390
PLUG, WOOD, REMOVABLE
SIZE D
DRAWING NUMBER 1013
SCALE 1/2
SHEET 1 OF 1
GEOMETRIC PRECISION - XXX.XXX XX

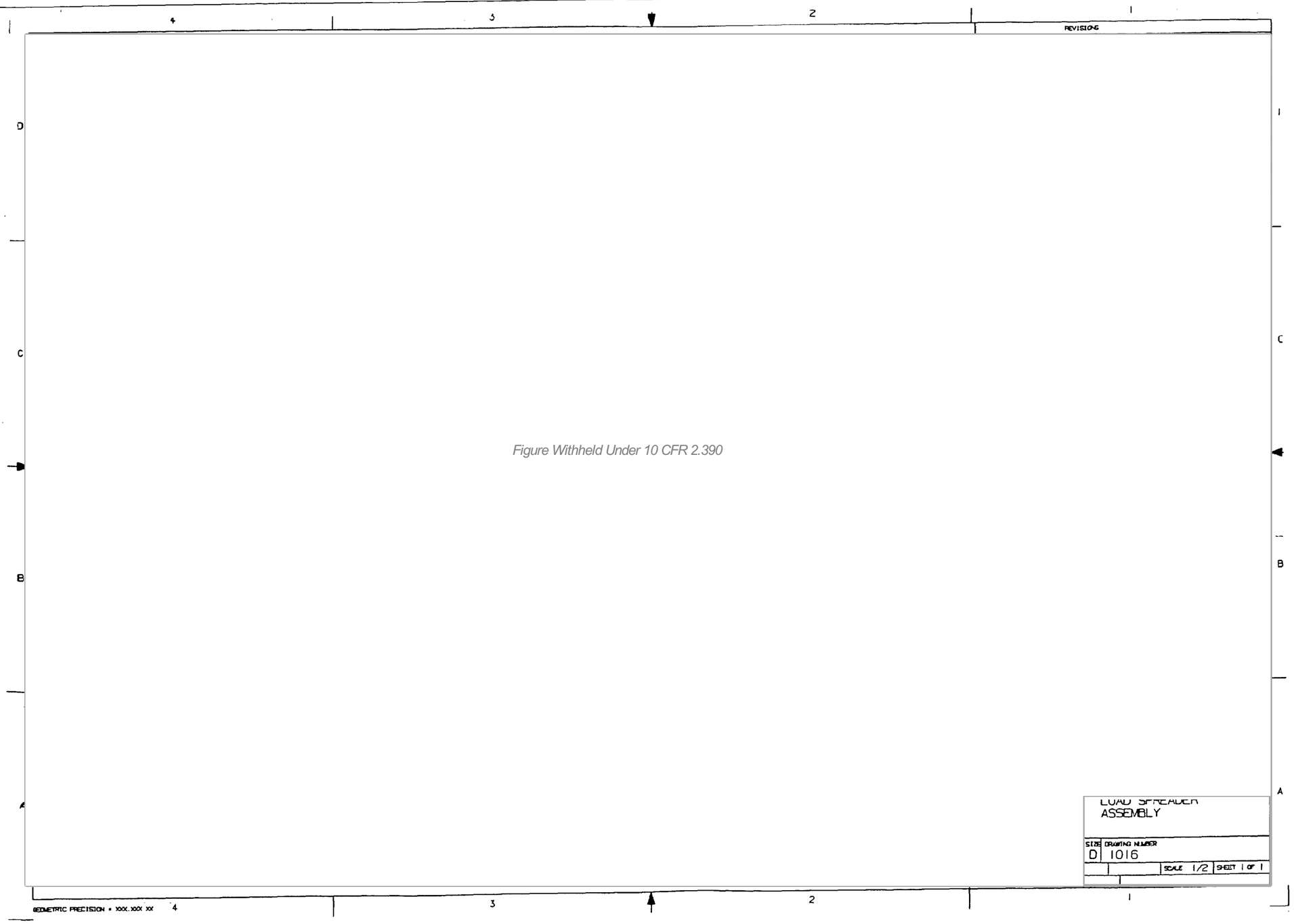

Figure Withheld Under 10 CFR 2.390

REVISIONS

Figure Withheld Under 10 CFR 2.390

CONTAINMENT VESSEL

SIZE DRAWING NUMBER D 1017 SCALE 1/1 SHEET 1 OF 1

GEOMETRIC PRECISION ± .XXX .XXX XX

Figure Withheld Under 10 CFR 2.390

BOLT, SOCKET, HEAD
SPECIAL .500-20

SIZE C | DRAWING NUMBER 1018 | SCALE 2/1 | SHEET 1 OF 1

GEOMETRIC PRECISION = XXX.XXX XX

Figure Withheld Under 10 CFR 2.390

GASKET COPPER

SIZE C | DRAWING NUMBER 1019 | SCALE 1/1 | SHEET 1 OF 1

GEOMETRIC PRECISION = XXX.XXX XX

Figure Withheld Under 10 CFR 2.390

Figure Withheld Under 10 CFR 2.390

Figure Withheld Under 10 CFR 2.390

Figure Withheld Under 10 CFR 2.390

TITLE
PAT-1/TB-1/T-AMPOULE
ASSEMBLY (U)

SIZE	DRAWING NUMBER	
E	R99794	
CAGEC 14213	SCALE NONE	SHEET 1 OF 1
ORIGIN SA-MST-V8		

RASTER FILE NOT TO SCALE

UNCLASSIFIED

UNCLASSIFIED

Figure Withheld Under 10 CFR 2.390

TB-1 / T-AMPOULE
SHIPPING VESSEL
ASSEMBLY (U)

SIZE	DRAWING NUMBER	ISSUE
D	2A0263	A

CAGEC 14213 SCALE 1/1 SHEET 1 OF 1

RE 2 STATUS SA-REL-08-13-09

UNCLASSIFIED

UNCLASSIFIED

UNCLASSIFIED

UNCLASSIFIED

Figure Withheld Under 10 CFR 2.390

BODY,
T- AMPOULE (U)

SIZE	DRAWING NUMBER	ISSUE
D	2A0259	A

CAGEC 14213 SCALE 1/1 SHEET 1 OF 1

IRE 2 STATUS SA-REL-08-21-09

UNCLASSIFIED

UNCLASSIFIED

UNCLASSIFIED

UNCLASSIFIED

Figure Withheld Under 10 CFR 2.390

TITLE: LID, T- AMPOULE (U)				
SIZE D	DRAWING NUMBER 2A0260			ISSUE A
	CAGEC 14213	SCALE 1/1	SHEET 1 OF 1	
IRE 2	STATUS SA-REL-08-13-09			

UNCLASSIFIED

UNCLASSIFIED

UNCLASSIFIED

UNCLASSIFIED

Figure Withheld Under 10 CFR 2.390

TITLE		
LID, T- AMPOULE (U)		
SIZE D	DRAWING NUMBER 2A0260	ISSUE A
	CAGEC 14213 SCALE 1/1	SHEET 1 OF 1
IRE 2	STATUS SA-REL-08-13-09	

UNCLASSIFIED

UNCLASSIFIED

UNCLASSIFIED

UNCLASSIFIED

Figure Withheld Under 10 CFR 2.390

T-AMPOULE
ASSEMBLY (U)

SIZE	DRAWING NUMBER	ISSUE
D	2A0261	A
	CAGEC 14213 SCALE 2/1	SHEET 1 OF 1
RE 2	STATUS SA-REL.-08-19-09	

UNCLASSIFIED

UNCLASSIFIED

UNCLASSIFIED

UNCLASSIFIED

Figure Withheld Under 10 CFR 2.390

TITLE		
RING, FILLER (U)		
SIZE D	DRAWING NUMBER 2A0262	ISSUE A
CAGEC 14213	SCALE 2/1	SHEET 1 OF 1
RE 2	STATUS SA-REL-08-13-09	

UNCLASSIFIED

UNCLASSIFIED

UNCLASSIFIED

UNCLASSIFIED

Figure Withheld Under 10 CFR 2.390

TITLE
BODY,
SAMPLE CONTAINER-1
(SC-1) (U)

SIZE	DRAWING NUMBER	ISSUE
D	2A0264	A
	CAGEC 14213 SCALE 2/1	SHEET 1 OF 1
RE 2	STATUS SA-REL-08-13-09	

UNCLASSIFIED

UNCLASSIFIED

UNCLASSIFIED

UNCLASSIFIED

Figure Withheld Under 10 CFR 2.390

SAMPLE CONTAINER-2
(SC-2)
ASSEMBLY (U)

SIZE	DRAWING NUMBER	ISSUE
D	2A0265	A
	CAGEC 14213 SCALE 2/1	SHEET 1 OF 1
IRE 2	STATUS SA-REL-08-19-09	

UNCLASSIFIED

UNCLASSIFIED

UNCLASSIFIED

UNCLASSIFIED

Figure Withheld Under 10 CFR 2.390

TITLE
BODY,
SAMPLE CONTAINER-2
(SC-2) (U)

SIZE	DRAWING NUMBER	ISSUE
D	2A0266	A
	CAGEC 14213 SCALE 2/1	SHEET 1 OF 1
RE 2	STATUS SA-REL-08-13-09	

UNCLASSIFIED

UNCLASSIFIED

UNCLASSIFIED

UNCLASSIFIED

Figure Withheld Under 10 CFR 2.390

TITLE
LID,
SAMPLE CONTAINER-1
(SC-1) (U)

SIZE	DRAWING NUMBER	ISSUE
D	2A0267	A
	CAGEC 14213 SCALE 2/1 SHEET 1 OF 1	
FIRE	STATUS SA-REL-08-13-09	

UNCLASSIFIED

UNCLASSIFIED

UNCLASSIFIED

UNCLASSIFIED

Figure Withheld Under 10 CFR 2.390

TITLE		
SAMPLE CONTAINER-1 (SC-1) ASSEMBLY (U)		
SIZE D	DRAWING NUMBER 2A0268	ISSUE A
	CAGEC 14213 SCALE 2/1	SHEET 1 OF 1
IRE 2	STATUS SA-REL-08-19-09	

UNCLASSIFIED

UNCLASSIFIED

UNCLASSIFIED

UNCLASSIFIED

Figure Withheld Under 10 CFR 2.390

TITLE	LID, SAMPLE CONTAINER-2 (SC-2) (U)
SIZE	D
DRAWING NUMBER	2A0269
ISSUE	A
CAGEC	14213
SCALE	2/1
SHEET	1 OF 1
IRE	
STATUS	SA-REL-08-13-09

UNCLASSIFIED

UNCLASSIFIED

UNCLASSIFIED

UNCLASSIFIED

Figure Withheld Under 10 CFR 2.390

INNER CRADLE (U)

SIZE	DRAWING NUMBER
D	2A0385

CAGE: 14213 | SCALE: 1/2 | SHEET: 1 OF 5

GRAPH: SolidWorks 2008

UNCLASSIFIED

UNCLASSIFIED

GEOMETRIC PRECISION ± 1/16 DTS415

UNCLASSIFIED

Figure Withheld Under 10 CFR 2.390

2A0385			
DRAWING CLASSIFICATION: UNCLASSIFIED			
SIZE D	CAGE 14213	SCALE 2/1	
	ISSUE A	SHEET 2 OF 5	
SCALE SA-REL-08/18/2009			

UNCLASSIFIED

UNCLASSIFIED

Figure Withheld Under 10 CFR 2.390

UNCLASSIFIED

DRAWING NUMBER	2A0385		
DRAWING CLASSIFICATION	UNCLASSIFIED		
SIZE D	CAGE 14213	SCALE 2/1	
	DWG A	SHEET 3 OF 5	
DATE SA-REL-08/18/2009			

UNCLASSIFIED

UNCLASSIFIED

UNCLASSIFIED

Figure Withheld Under 10 CFR 2.390

2A0385

UNCLASSIFIED

D | CAGE: 14213 | SCALE: 2/1

A | SHEET: 4 OF 5

STATUS: SA-REL-08/18/2009

UNCLASSIFIED

UNCLASSIFIED

UNCLASSIFIED

UNCLASSIFIED

Figure Withheld Under 10 CFR 2.390

DRAWING NUMBER	2A0385		
DRAWING CLASSIFICATION	UNCLASSIFIED		
SIZE D	CAGE 14213	SCALE 2/1	
	SIZE A	SHEET 5 OF 5	
STATUS	SA-REL-08/18/2009		

UNCLASSIFIED

UNCLASSIFIED

1.3.3 Specifications

The following subsection includes the specifications for procuring titanium and O-ring materials.

1.3.3.1 PAT-1040 Titanium and O-Ring Materials and Component Fabrication Specification

See stand-alone document below.

PAT-1040 Titanium and O-Ring Materials and Component Fabrication Specification

Sandia National Laboratories

August 3, 2009

Prepared by: Richard H. Yoshimura Date: August 13, 2009
Richard H. Yoshimura, PAT-1 Project

Reviewed by: _____ Date: 8-19-2009
Perry L. Jones, QA Coordinator

Approved by: David R. Miller Date: 8/19/2009
David R. Miller, Manager

Revision Log

Revision No.	Date	Description of Change
0	August 3, 2009	Original Release

1 General

1.1 Summary

This fabrication specification establishes the quality, workmanship requirements and defines how quality is measured for the titanium components and procured parts within the Plutonium Air Transportable Package (PAT-1). The titanium components serve as a eutectic barrier, plutonium metal packaging containers, and support cradle for sample containers. This specification defines the titanium 6Al-4V (Ti-6Al-4V) Grade 5 material specification for the fabrication of the *T-Ampoule; Ring, Filler; Sample Container-1 (SC-1) Assembly; Sample Container-2 (SC-2) Assembly; Inner Cradle* and the procurement requirement for the *O-rings.* ASTM material specifications for the Ti-6Al-4V Grade 5 bar or sheet stock include minimum requirements specified in Section 3.1 of this document.

1.2 Definitions

Terms and Definitions

Certified Material Test Report - A document attesting that the material is in accordance with specified requirements, including actual results of all required chemical analyses, mechanical tests, and examinations. In addition to technical data, the document shall contain the SNL purchase order number, manufacturer or testing agency name and address and shall be signed by an authorized company representative.

Certificate of Conformance - A document signed and otherwise authenticated by an authorized company representative certifying the items meet all specified requirements.

Nonconformance - A deficiency in characteristic or documentation that renders the quality of an item unacceptable or indeterminate.

1.3 Abbreviations/Acronyms

Term	Description
ASNT	American Society for Nondestructive Testing
ASTM	American Society for Testing and Materials
CMTR	Certified Material Test Report
COC	Certificate of Conformance
SNL	Sandia National Laboratories
SAE	Society of Automotive Engineers
QAP	Quality Assurance Program

1.4 Requirements Documents

Unless otherwise approved, the following codes and standards (latest issue at the time of work) shall apply to establish the applicable minimum requirements for the titanium components and elastomeric O-rings. Reference test methods, specifications, and recommended practices are to be used to verify material properties and identify acceptable practices applicable to titanium and

O-ring components. Failure to identify applicable codes and standards does not imply elimination of required knowledge and compliance to perform work.

Document Number	Document Title
ASME Y14.5M	Dimensioning and Tolerancing
ASME BPVC	American Society of Mechanical Engineers (ASME); Boiler and Pressure Vessel Code, Section VIII Division 1, Rules for Construction of Pressure Vessels, 2007.
ASME BPVC	American Society of Mechanical Engineers (ASME); Boiler and Pressure Vessel Code, Section II Materials Part D Properties (Customary), 2007.
ASNT TC-1A	Recommended Practice for Personnel Qualification and Certification of Nondestructive Testing
ASTM B 348 (latest version)	Standard Specification for Titanium and Titanium Alloy Bars and Billets
ASTM B 265 (latest version)	Standard Specification for Titanium and Titanium Alloy Strip, Sheet and Plate
MIL-HDBK-5J*	Department of Defense Handbook, Metallic Materials and Elements for Aerospace Vehicle Structures," 31 January 2003.
SAE AMS-R-83248/1	Rubber, Fluorocarbon Elastomer, High Temperature, Fluid, and Compression Set Resistant (O-rings, Class 1, 75 Hardness
SAE AS568C	Aerospace Size Standard for O-rings
SAE AMS 2801B	Heat Treatment of Titanium Alloy Parts

1.5 Reference Documents

Document Number	Document Title
Ring, Filler	2A0262
T-Ampoule Assembly	2A0261
Sample Container-1 (SC-1) Assembly	2A0268
Sample Container-2 (SC-2) Assembly	2A0265
Inner Cradle	2A0385
O-ring, Viton, for T-*Ampoule Assembly*	2A0261, Item 3
O-ring, Viton, for *SC-1* and *SC-2*	2A0268, Item 3; 2A0265, Item 3

1.6 Technical Submittals

All required submittals stated in this specification shall be submitted to SNL for review and documented approval in accordance with Section 4.6 Documentation, which present a summary of Subcontractor/Supplier submittal requirements. Submittals that do not meet the project requirements shall be rejected. Rejected submittals shall be corrected and resubmitted in a timely manner to avoid delays.

* This document is still available and used by industry.

2 *Quality Assurance Requirements*

The quality assurance requirements are set forth in Section 9 of the PAT-1 Addendum and shall be incorporated in the procurement.

2.1 Quality Assurance Program

The vendor's QAP shall describe systems for planning, performing, and assessing work, which ensure materials, systems, results, and personnel meet stated quality objectives. The vendor shall qualify and approve any material suppliers and subcontractors utilized during the performance of the contract to the vendor's QAP. The vendor shall pass down all applicable QA requirements to any subcontractors. The vendor's QAP shall be submitted to SNL for review and written approval prior to the start of any work. Other quality requirements (audits and assessments, access to vendor facilities, on-site inspection and witnessing, qualification of vendor inspectors, nonconformance reporting, receiving and inspection, CMTRs, and COCs) apply per the contract documentation.

2.2 Evaluation and Approval

The supplier shall be evaluated and approved to furnish precision machining, metal fabrication, and assembly of components by SNL prior to contract award.

2.3 Audits and Assessments

SNL reserves the right to audit and assess the Supplier and Supplier's subcontractors and suppliers to verify conformance to the quality assurance program prior to the award of the contract, and at any time during performance of the contract.

Access to Supplier Facilities

SNL reserves the right to have its own qualified inspectors and personnel present during fabrication and inspection activities. At least five working days notice is required prior to inspection and testing activities planned by the Supplier so SNL can arrange for its staff's participation. Hold points may be identified in the schedule for coordination of inspection activities.

2.4 Qualification of the Supplier's Inspectors

Inspectors shall be suitably experienced and qualified. Inspectors independent of the operation shall carry out acceptance inspections.

2.5 Nonconformance Reporting

Nonconforming items are to be reported as outlined in the Supplier's approved QAP, with immediate written notification to SNL. Nonconformance Reports (NCR) shall be compiled to document the details of the nonconformance. Any nonconforming components shall be clearly identified and segregated. NCRs shall be traceable to actual components(s) affected. SNL shall disposition "Use-As-Is", "Repair", or "Reject" nonconforming items in writing prior to the

Supplier proceeding with the next activity or step in the fabrication process. A copy of the completed NCR shall be submitted to SNL by the Supplier as part of the manufacturing documentation for "Use-As-Is" or "Repair" dispositions.

2.6 Receiving and Inspection

Upon delivery to SNL, the parts will be dimensionally and visually inspected by SNL authorized receipt inspectors as follows:

- Visually inspect components and assemblies for damage
- Verify purchase order number is marked on the parts, packaging, or accompanying documentation
- Verify CMTR contains manufacturer or testing agency name and address, and is signed by an authorized company representative
- Verify COC provided for each individual or lot of components
- Verify COC contains SNL purchase order, Supplier name and address and is signed by an authorized company representative

3.0 Materials

3.1 Titanium Components

3.1.1 Specific Material Requirements - ASTM requirements for the Ti-6Al-4V Grade 5 material are specified except minimums are specified for yield strength, ultimate tensile strength, elongation at tensile failure, reduction of area at failure. In some cases, heat treating may be required to meet the requirement of the solution treated and aged (STA) condition. The following presents specific material requirements for the titanium materials required for the following components:

Component	Specification
• T-Ampoule Assembly, 2A0261	Procure Ti-6Al-4V material meeting requirements of ASTM B-348 Grade 5 (use latest version for all documents), rough machine to drawing dimensions, leaving 0.05"+/-0.01" machining allowance on all surfaces. The titanium parts shall be protected from iron contamination before and during heat treatment. Heat treat to MIL-HDBK-5J strength requirements* for STA condition per requirements and procedures of SAE AMS 2801B. Finish machine to drawing dimensions.

* If material purchased already meets the requirements for the STA condition, the rough machine and heat treatment parts of the procedure stated above are not necessary.

Component	Specification
• Ring, Filler, 2A0262 • Sample Container-1 (SC-1) Assembly, 2A0268 • Sample Container-2 (SC-2) Assembly, 2A0265 • Inner Cradle, 2A0385: (Components) o 2A0385-025 Dish in Lid o 2A0385-020 Dish in Body o 2A0385-010 Leg (4 each) o 2A0385-015 Upper Leg (4 each) o 2A0385-030 Lock Ring (2 each)	Procure Ti-6Al-4V material meeting requirements of ASTM B-265 Grade 5, except with minimum values as follows: 0.2% yield strength: 140 ksi; ultimate tensile strength: 150 ksi; elongation at tensile failure: 10%; reduction of area at failure 20%.
• Inner Cradle, 2A0385: (Components) o 2A0385-045 Spacer (2 each for SC-2) o 2A0385-040 Spacer (3 each for SC-1).	Procure Ti-6Al-4V material meeting requirements of ASTM B-348 Grade 5, except with minimum room temperature values as follows: 0.2% yield strength: 140 ksi; ultimate tensile strength: 150 ksi; elongation at tensile failure: 10%; reduction of area at failure 20%.

3.1.2 The CMTR for the titanium material used to fabricate the titanium components shall be submitted for SNL approval prior to the start of fabrication activities.

3.2 Elastomeric O-Ring Seals

3.2.1 The elastomeric compound material used to manufacture all O-ring seals shall be Parker Compound Number "V0747-75" conforming to SAE AMS-R-83248/1, *Rubber, Fluorocarbon Elastomer, High Temperature, Fluid, and Compression Set Resistant* (O-rings, Class 1, 75 Hardness), August 1, 2000.

3.2.2 The manufacturing tolerances for furnished O-ring seals shall conform to SAE AS 598C, *Aerospace Size Standard for O-rings*.

3.2.3 O-ring vendor shall provide a COC verifying that O-ring seals conform to the specifications above with the construction report. SAE AS568C provides standards on O-ring dimensions.

4.0 Fabrication Requirements

4.1 Equipment

The machine shop performing this fabrication shall supply all tooling, fixtures, and machines necessary to meet the fabrication requirements.

4.2.1 Inspection and Examination Requirements

Qualified and certified inspectors meeting the requirements of ASNT TC-1A shall perform all inspections.

4.2.2 A full dimensional inspection of the hardware shall be performed and documented to assure adherence to the dimensions and associated tolerances in the engineering drawings. ASME Y14.5M, *Dimensioning and Tolerancing*, shall serve as the basic standard for the dimensional inspection.

4.3 Product Marking

Vendor shall mark the product, packaging and accompanying documentation with the Item's part number. Laser marking is required on all metal part areas identified in the engineering drawing set (2A0259, 2A0260, 2A0261, 2A0262, 2A0264, 2A0265, 2A0266, 2A0267, 2A0268, 2A0269, 2A0385).

4.4 Surface Finish

All titanium surfaces shall be cleaned to remove grease, oil, salt, chemicals, etc. prior to packaging. The cleaning operation shall not use abrasives, and all machined surfaces shall be protected from damage.

O-ring seal areas will meet specific surface finish requirements as set out on the fabrication drawings.

4.5 Packaging and Shipping Requirements

Items fabricated to this technical specification shall be packaged to prevent damage during shipping or transport to SNL.

4.6 Documentation

The Supplier shall submit a formal construction report to SNL for review and written approval prior to shipment. The construction report shall contain the minimum documentation listed below and a minimum of three copies of the required document submittals.

The construction report shall contain the following documentation at a minimum:

- Vendor's Quality Assurance Program Manual
- CMTRs for procured raw materials including stress strain curves, heat treatment
- Certificates of Conformances for procured components
- Certificated of Conformance for fabricated T-Ampoule; Ring, Filler; Sample Container-1; Sample Container-2; Inner Cradle and O-rings.

- Product Travelers
- Qualifications and Certifications of Personnel Performing Inspection Activities
- Inspection Records
- Engineering Change Notices, Design Deviation Requests or similar documents
- Non-Conformance Reports
- Construction Report

5.0 Requirements Specific to the T-Ampoule Titanium Components Fabrication and Inspection

With the exception of the elastomeric (O-ring) seal, the T-Ampoule (Drawing 2A0261) was designed, will be fabricated and will be inspected to meet the requirements of the ASME Boiler and Pressure Vessel Code (Section VIII) with the following exceptions or explanations:

1. The T-Ampoule meets the requirements of Section VIII as modified by this document.
    a. The size requirements of section *U-1(c)(2)(i)* of Section VIII do not apply.
    b. The marking requirements of parts UG 115-119 do not apply. T-Ampoules will be marked with part and serial numbers.
2. Given the dry inert gaseous initial atmosphere and the general non-reactivity of titanium with vessel contents, design calls for no corrosion allowance.
3. T-Ampoule MAWP will be established by calculations as set forth in this document. Allowable pressure calculations will be performed based on the following paragraphs of Section VIII:
    a. Torispherical Head allowable pressure is calculated based on the requirements of Section VIII's Mandatory Appendix 1, Supplementary Design Formulas, paragraph 1-4(d).
    b. Allowable pressure, based on membrane stress in the hemispherical head, is estimated based on the criteria set forth in paragraph UG-32.
    c. Allowable pressures in both the longitudinal and circumferential direction of the shell and lid are estimated based on the criteria set forth in paragraph UG-27.
    d. T-Ampoule is exempt from the requirements of paragraph UG 32, *Thickness of Shells and Tubes Under External Pressure*. As the T-Ampoule will be subject to impact loading a separate impact analysis will be conducted as described in Section 2 of the document PAT-1 Safety Analysis Report Addendum Docket No. 71-0361, Rev. 0, August 2009.

e. Since no welded joints exist on the T-Ampoule, joint efficiency, E, in all Section VIII equations were taken as 1.0.

4. The requirements of paragraph UG-125 regarding pressure relief devices do not apply. Overpressure response will be discussed in detail in the body of this paper.

5. T-Ampoule will be fabricated of Ti-6Al-4V titanium alloy produced to the specifications in Section 3.1 of this specification except as modified below.

    a. Temperature-dependent allowable stress criteria will be determined using the procedures outlined in the ASME Boiler and Pressure Vessel Code, Section II Part D, *Mandatory Appendix 1 Basis for Establishing Stress Values in Tables 1A and 1B.*

    b. In either case, titanium maintains ductility at low temperatures and is therefore exempt from the requirements of Sections UCS 66 through 68 pertaining to derating allowable stress for low-temperature operation.

6. In the case of analysis of the torispherical heads, and in accordance with Section UG-32(e), allowable stress will be limited to 20,000 psi for temperatures below 77°F, and will be reduced proportional to the curves developed in 2.b above for temperatures above 77°F.

7. In addition to the quality requirements of Section 2 of this specification, the T-Ampoule quality program will meet the requirements of Section VIII with the following exceptions:

    a. The standard hydrostatic test of paragraph UG-99 or the pneumatic test of paragraph UG-100 are not required.

    b. The requirements of paragraph UF-55 regarding ultrasonic examination do not apply. Inspection will consist of visual inspection and physical measurement of specified dimensions.

    c. As the T-Ampoule components are machined without welding, the requirements of part UW and part UB do not apply.

    d. In lieu of the requirements of paragraph UG-91, the inspector will meet the requirements listed below:

        i. Inspector will demonstrate experience with spinning and fabrication processes.

        ii. Inspector will demonstrate experience with Section VIII.